CD8+ T-cells in atherosclerosis: recognizing their contribution

Jong, M.J.M. de


3

Chapter 3

Resident memory T-cells in the atherosclerotic lesion associate with reduced macrophage content and increased lesion stability

Authors: M.J.M. de Jong[1], M.A.C. Depuydt[1], F.H. Schaftenaar[1], K. Liu[1], D. Maters[1], Anouk Wezel[3], Harm J. Smeets[3] J. Kuiper[1], I. Bot[1], K. van Gisbergen[2], B. Slütter[1]

1 Leiden Academic Centre for Drug Research, Division of BioTherapeutics, Leiden University, Einsteinweg 55, 2333 CC Leiden, The Netherlands.
2 van Gisbergen Lab, Tissue Immunity, Champalimaud research, Lisbon, Portugal
3 Department of Surgery, Haaglanden Medical Center, The Hague, The Netherlands.

Published in Arteriosclerosis, Thrombosis, and Vascular Biology, 2024 Apr 18,
https://doi.org/10.1161/ATVBAHA.123.320511

ABSTRACT

Introduction. Tissue-resident memory T-cells (T_{RM}) are a T-cell subset that resides at the site of prior antigen recognition to protect the body against recurring encounters. Besides their protective function, T_{RM} have also been implicated in inflammatory disorders. T_{RM} cells are characterized by the expression of CD69, and transcription factors Hobit and Blimp-1. As the majority of T-cells in the arterial intima express CD69, T_{RM} may contribute to the pathogenesis of atherosclerosis as well. Here, we aimed to assess the presence and potential role of T_{RM} cells in atherosclerosis.

Methods. To identify T_{RM} cells in human atherosclerotic lesions, a single-cell RNA sequencing dataset was interrogated, and T-cell phenotypes were compared to that of integrated predefined T_{RM} cells. The presence and phenotype of T_{RM} in atherosclerotic lesions was corroborated using a mouse model that enabled tracking of Hobit-expressing T_{RM} cells. To explore the function of T_{RM} during atherogenesis, *Rag1*$^{-/-}$*Ldlr*$^{-/-}$ mice received a bone marrow transplant from Hobit$^{KO/CRE}$Blimp-1$^{flox/flox}$ mice, which exhibit abrogated T_{RM} formation, whereafter the mice were fed a Western-type diet for 10 weeks.

Results. Human atherosclerotic lesions contained T-cells that exhibited a T_{RM} associated gene signature. Moreover, a fraction of these T-cells clustered together with predefined T_{RM} cells upon integration. The presence of Hobit-expressing T_{RM} cells in the atherosclerotic lesion was confirmed in mice. These lesion-derived T_{RM} were characterized by the expression of CD69 and CD49α. Moreover, we demonstrated that this small T-cell subset significantly affects lesion composition, by reducing the amount of intralesional macrophages and increasing collagen content.

Conclusion. T_{RM} cells, characterized by the expression of CD69 and CD49α, constitute a minor population in atherosclerotic lesions, and associated with increased lesion stability in a Hobit and Blimp-1 knockout mouse model.

HIGHLIGHTS

- A small fraction of resident memory T-cells is detected in human atherosclerotic lesions.
- In murine atherosclerotic lesions T_{RM} cells express CD69^{+}CD49α^{+}.
- Deletion of T_{RM} associated with a reduced amount of intralesional macrophages and increased collagen content.

KEYWORDS: Atherosclerosis, Resident memory T-cells (T_{RM}), T-cells, CD69, Immunology

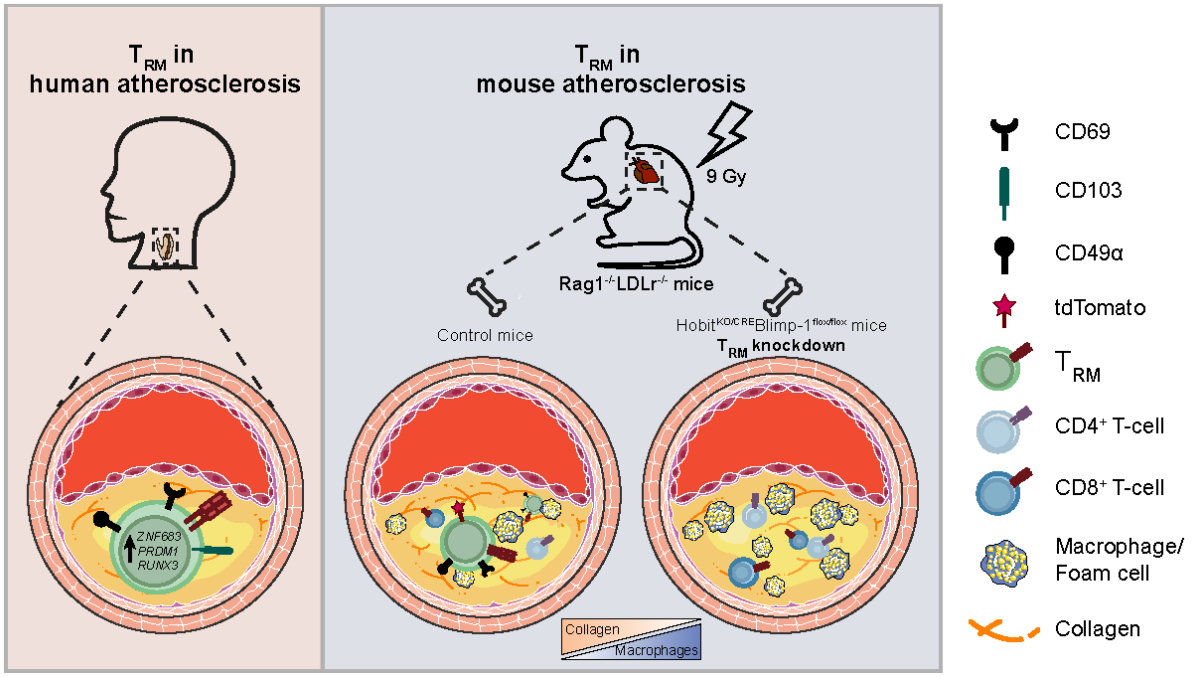

Grapical abstract

INTRODUCTION

Atherosclerosis is a lipid-driven chronic inflammatory disease of the larger arteries resulting in vascular occlusion with clinical complications, including stroke and myocardial infarction. Various immune cell types inside the atherosclerotic lesions have been extensively studied, including T-cells. Recent single-cell sequencing and cytometry techniques have identified T-cells as one of the main immune cell populations in human and mouse atherosclerotic lesions[1–4]. Both $CD4^+$ and $CD8^+$ T-cells are highly represented and exhibit a heterogeneous phenotype within the atherosclerotic lesion, encompassing distinct T-cell subsets and memory phenotypes[1,2,5].

Interestingly, plaque-residing T-cells demonstrate significantly elevated CD69 expression compared to circulating T-cells, with approximately 60% of all T-cells in the plaque expressing this molecule[6]. CD69 is a transmembrane C-type lectin, and is upregulated upon TCR stimulation, but can also be induced by other external stimuli such as exposure to type I IFN[7]. CD69 is involved in a variety of cellular processes, including proliferation and signal transduction, and controls tissue retention by regulating sphingosine-1-phosphate receptor 1 (S1PR1) expression[8]. Based on its function, CD69 can be used as a marker for early TCR activation as well as for tissue residency in T-cells.

Tissue-resident memory T-cells (T_{RM}) reside at the site of previous antigen encounter without access to the circulation, and are primed to provide rapid and localized immune responses upon interacting with familiar antigens. Although T_{RM} are very efficient in countering secondary infections, they have also been implicated in the involvement of chronic inflammatory diseases. T_{RM} are often enriched at sites of chronic inflammation[9,10]. Moreover, multiple studies have demonstrated the involvement of T_{RM} in recurring disease flares[10,11]. For example, in rheumatoid arthritis, disease recurrence was ameliorated by depleting T_{RM} cells[11] .

Yet, the involvement of T_{RM} cells in atherosclerosis remains elusive. T-cells exhibiting a T_{RM}-like phenotype have been identified in human and mouse atherosclerotic lesions, and $CD69^+$ $CD103^+$ $CD8^+$ T-cells with a T_{RM}-like phenotype were specifically expressed in human atherosclerotic lesions, but not in blood[2,12]. Moreover, the majority of the T-cells in the atherosclerotic lesion have an effector memory phenotype, combined with high expression of CD69 ($CCR7^{low}CD45RA^{high}CD69^+$)[1,2,13]. On the other hand, Depuydt et al. (2023) demonstrated that these $CD69^+$ effector memory T-cells show signs of clonal expansion and recent TCR activation, arguing that T-cells in the lesion can also express CD69 as a result of antigen recognition[6].

In this study, we aimed to assess the phenotype, proportion, and function of T_{RM} in the atherosclerotic lesion. To interrogate the phenotype of T-cells in the lesion, we used scRNAseq data of human atherosclerotic lesions, and performed FACS analysis for T_{RM} associated molecules on lymphocyte preparations isolated from mouse atherosclerotic lesions. To evaluate the proportion and function of T_{RM} in atherosclerotic lesions, a bone marrow transplantation study was performed, in which the formation of T_{RM} cells was hindered.

MATERIALS AND METHODS

The data that support the findings of this study are available from the corresponding author upon reasonable request.

Human studies. Handling of all human samples complied with the "Code for Proper Secondary Use of Human Tissue" and was in accordance with the declaration of Helsinki regarding ethical principles for medical research involving human subjects and all patients signed an informed

consent form. To evaluate the proportion of T_{RM} marker expressing T-cells in the atherosclerotic lesion, atherosclerotic plaques samples were obtained from 20 patients who underwent carotid endarterectomy surgery (CEA) at the Haaglanden Medical Center, Westeinde, The Hague, Netherlands (Study approval number: 17-046, protocol number NL57482.098.17). Only atherosclerotic plaques from primary CEA's were included in this study.

Human atherosclerotic plaque cell isolation. Human endarterectomy samples were digested into a single-cell suspension following a previously described protocol[6]. In brief, lesions were digested into a single-cell suspension by cutting the tissue into pieces of approximately 1 mm^2, followed by digestion with 2.5 mg/mL Collagenase IV (ThermoFisher Scientific), 0.25 mg/mL DNAse I (Sigma), 2.5 mg/mL Human Albumin Fraction V (MP Biomedicals) in RPMI 1640 for 30 minutes at 37°C. After digestion, plaque tissue was mashed over a 70 µm strainer to create a single-cell suspension and washed in RMPI 1640. Cells were cryostored in Cryostor cell cryopreservation medium (Sigma-Aldrich) at -80°C until further use.

Single-cell RNA sequencing on human plaques. An previously published single-cell RNA sequencing (scRNAseq) data set was used to interrogate the phenotype of T_{RM} cells in the atherosclerotic lesion[6]. In brief, scRNAseq was performed on PBMCs and atherosclerotic lesions of 3 male patients who underwent carotid endarterectomy. PBMCs and single-cell plaque suspensions were stained with TotalSeq-C antibodies against CD3 and CD14. Plaque suspensions were additionally stained for CD45. ScRNA-seq was performed on PBMCs and live $CD45^+$ plaque cells, using 10x Genomics 5′ Single-cell Immune Profiling technology. Next, $CD3^+$ T-cells were selected from all immune cells and subclustered.

Integration of T_{RM} dataset. To compare the phenotype of plaque-residing T-cells with T-cells previously identified as T_{RM}, T_{RM} cells were selected from a published scRNAseq dataset containing gene expression data of T-cells from human intestinal transplants, and integrated with the plaque T-cells, following the Seurat "introduction to scRNAseq integration" vignette [14]. In brief, raw data (Gene Expression Omnibus: GSE162687) was processed using Seurat omitting cells with gene expression <200 and >2500, or >10% mitochondrial genes from the dataset.

In order to decrease the dimensionality of the normalized data and execute cell clustering, a principal component analysis (PCA) was conducted. The initial 10 PCA components were utilized for identifying clusters at a resolution of 0.4, following the authors' description.

After integration of the predefined T_{RM} into the atherosclerosis dataset, the curated dataset was clustered based on the top 15 PCA components, and a resolution 0.7. Next, classical T_{RM}, with high expression of *CD69*, *ITGAE* and *ZNF683,* were selected from the integrated T_{RM} dataset for projection onto and integration into the atherosclerosis scRNAseq dataset. Other T-cells from the integrated dataset were removed from the curated dataset. Clusters were visualized using UMAP, and annotated based on differential gene expression between clusters, identified by a Wilcoxon Rank Sum test (FindMarkers function Seurat).

T_{RM} gene signature. T_{RM} gene signature was based on the core signature of T_{RM} cells previously described by Kumar et al. (2017)[15] and the canonical transcription factors involved in T_{RM} differentiation. The signature included: "CD69", "CA10", "ITGA1", "ITGAE", "IL2", "IL10", "CXCR6", "CXCL13", "KCNK5", "RGS1", "CRTAM", "DUSP6", "PDCD1", "ZNF683", "PRDM1", and "RUNX3". The AddModuleScore function was used to calculate the average expression level of the genes included in the T_{RM} gene signature.

Animals. C57BL/6J , RAG1 deficient (*Rag1*$^{-/-}$) and LDL receptor knockout mice (*Ldlr*$^{-/-}$) mice were purchased from The Jackson Laboratory (Sacramento, CA, USA) and bred in-house. Animals were kept under standard laboratory conditions and food and water were provided *ad libitum*. All animal work was performed in female mice, to prevent sex-driven variation in atherosclerosis development. All work was in compliance with the Dutch government guidelines and the Directive 2010/63/EU of the European Parliament and experiment were approved by the Ethics Committee for Animal Experiments and the Animal Welfare Body of Leiden University (Project 106,002,017,887, Study number 887,3–178).

Donor mice. During the bone marrow transplant experiments we used wildtype mice (C57BL/6J mice), Hobit^{tdTomato} mice (B6-Tg(Zfp683-tdTomato-P2A-Cre-P2A-DTR)[16], bone marrow obtained from Sanquin Research), and Hobit$^{KO/CRE}$Blimp-1$^{flox/flox}$ mice (Hobit$^{CRE/tdTomato}$ x Blimp-1$^{flox/flox}$, bone marrow obtained from Sanquin Research[17,18]) as donor mice. Hobit^{tdTomato} mice exhibit one functional *Zfp683* allele, allowing normal Hobit regulation, and one dysfunctional allele, in which *Zfp683* has been replaced for a cassette containing tdTomato, CRE recombinase and DTR genes separated by P2A sequences enabling tracking and manipulation of Hobit-expressing cells [16]. Hobit$^{KO/CRE}$Blimp-1$^{flox/flox}$ mice, have two disrupted *Zfp683* alleles[17,18]. One allele has been replaced with the tdTomato-P2A-Cre-P2A-DTR cassette, while the other allele has been disrupted with a gene-trapping construct. *Zfp683*-induced expression of Cre recombinase leads to the excision of the LoxP flanked exon 6 of the *Prdm1* gene, resulting in dysfunctional Blimp-1 in cells with an active *Zfp683* locus and therefore preventing the formation of T_{RM} cells. This *Zfp683*-Cre floxed *Prdm1* system knocks out Blimp-1 with 80% efficiency.

Bone marrow transplant. 45 female *Rag1*$^{-/-}$*Ldlr*$^{-/-}$ mice of 8-16 weeks of age were exposed to 9 Gy (2x 4,5 Gy, 0.19 Gy/min, 200 kV, 4 mA) total body irradiation using an Andrex Smart 225 Röntgen source (YXLON International) with a 6-mm aluminum filter to induce bone marrow aplasia. Mice received 10*10^6 donor bone marrow cells originating from either wildtype mice (C57BL/6 mice), Hobit^{tdTomato} mice (Hobit$^{+/tdTomato}$ mice, bone marrow obtained from Sanquin laboratories), or Hobit$^{KO/CRE}$Blimp-1$^{flox/flox}$ mice (Hobit$^{CRE/tdTomato}$ x Blimp$^{flox/flox}$, bone marrow obtained from Sanquin laboratories) in 100 µl saline via tail vein injection. Bone marrow was isolated by flushing the femoralis and tibia with PBS and passing the cells through a 70 µm cell strainer (Greiner Bio-One). During the recovery period of 4 weeks, the drinking water of the mice was supplemented with antibiotics (83 mg/L ciprofloxacin, 67 mg/L polymyxin B sulfate, and 6.5 g/L sucrose). After recovery, the mice were fed a Western-type diet (0.25% cholesterol and 15% cacao butter (Special Diet Services)) for 10 weeks to induce lesion formation. Upon sacrifice the mice were anesthetized intraperitoneally with mix of ketamine (100 mg/mL), Xylazine (10 mg/mL). Blood was collected via orbital bleeding, followed by perfusion with PBS through the left ventricle. Heart, aorta, spleen and liver were collected for further analysis.

Organ processing. Single-cell suspensions of the spleen and liver were obtained by using a 70 µm cell strainer (Greiner Bio-One). Red blood cells were removed from liver, spleen and blood samples by lysing the red blood cells for 2 minutes at room temperature with lysis buffer. To separate leukocytes from hepatocytes in the liver samples, gradient centrifugation with 35% Percoll (Merck) was applied. Aortas were cut into small fragments of approximately 1 mm^2, and incubated with a digestion mix of (collagenase I 450 U/mL, collagenase XI 250 U/mL, DNAse 120 U/mL and hyaluronidase 120 U/mL; all Sigma-Aldrich) for 30 minutes at 37˚C while rotating. Digested aorta samples were passed over a 70 µm cell strainer to obtain a single-cell suspension. The upper part of the heart were embedded in Tissue-Tek OCT (Sakura) and stored at -80 ˚C until further usage.

Cholesterol assay. Serum was obtained by collecting whole blood in clot-inducing microvette CB300Z tubes (Sarstedt), followed by centrifugation at 2000 RCF for 10 minutes at 4°C. Serum was stored at -80°C until further usage. Total cholesterol levels in serum were measured by performing a enzymatic colorimetric analysis (Roch/Hitachi, Germany), using Precipath standardized serum (1.69 mg/ml, Roche/Hitachi) as an internal standard.

Flow cytometry. Approximately 500,000 cells, or all available cells, were stained with the appropriate antibodies (supplementary table I), Fc block (Biolegend), and live/dead viability staining (eBioscience) in PBS containing 2% FCS for 30 minutes at 4°C. Prior to intracellular staining, the cells underwent fixation and permeabilization using an intracellular staining kit (eBioscience) or an intranuclear staining kit (FOXP3/Transcription factor staining buffer set, eBioscience), following the manufacturer's instructions. To assess cytokine production, the cells were stimulated for 4 hours with phorbol 12-myristate 13-acetate (PMA, 50 ng/mL, Sigma-Aldrich) and ionomycin (500ng/mL, Sigma-Aldrich) in the presence of brefeldin A (5 µg/ml, ThermoScientific) in complete RPMI at 37°C and 5% CO_2. Flow cytometry measurements were performed on a Cytoflex S (Beckman Coulter). Data analysis was performed using FlowJo v10.7 software (Treestar). Gating strategies are visualized in supplemental Figure 7-9. For the identification of T_{RM} in human atherosclerotic lesions, samples with <50 $CD4^+$ or $CD8^+$ T-cells were excluded.

Histological analysis. The trivalve area of the hearts were sectioned at 7 µm thickness using a Leica CM1950 cryostat. The size of atherosclerotic plaques and the percentage of stenosis were determined using Oil-Red-O (ORO) staining (Sigma-Aldrich). To assess collagen content and necrotic core size in the atherosclerotic lesions, Masson's trichrome staining (Sigma-Aldrich) was performed. To determine macrophage content in the lesions, sections were immunohistochemically stained with a primary antibody targeting a macrophage-specific antigen (MOMA-2, monoclonal rat IgG2b, diluted 1:1000), followed by secondary antibody staining with biotinylated rabbit anti-rat IgG (BA-4001, Vector, dilution 1:200). The reaction was visualized using ImPACT NovaRED Peroxidase (HRP) substrate (Vector). All sections were digitized using a Panoramic 250 Flash III slide scanner (3DHISTECH, Hungary). Data analysis were performed using ImageJ software.

Statistical analysis. Data analysis was performed using Prism 9.0 (GraphPad Software, Inc. San Diego, CA, USA). Data are expressed as mean ± SD for all analyses. Outliers were identified by a ROUT or Grubbs outlier test. Shapiro-Wilkson normality test was used to test data for normal distribution. Normally distributed data was analyzed using a two-tailed unpaired student's T-test when comparing two groups, or a two way ANOVA with Bonferroni's multiple comparisons test when comparing two groups with multiple conditions. Not-normally distributed data was analyzed using a Mann-Whitney test. Statistical analysis were performed using GraphPad Prism. Probability values of $P = < 0.05$ were considered to be significant.

To evaluate differential gene expression between T_{RM}-like T-cells in the atherosclerotic lesion and other lesion-derived T-cells, the FindMarkers function was used. Differential gene expression was computed using a non-parametric Wilcoxon rank-sum, and Bonferroni-corrected P-values were determined considering the overall gene count in the dataset. Visualization of the differential gene expression was carried out using a Volcano plot, facilitated by the EnhancedVolcano package.

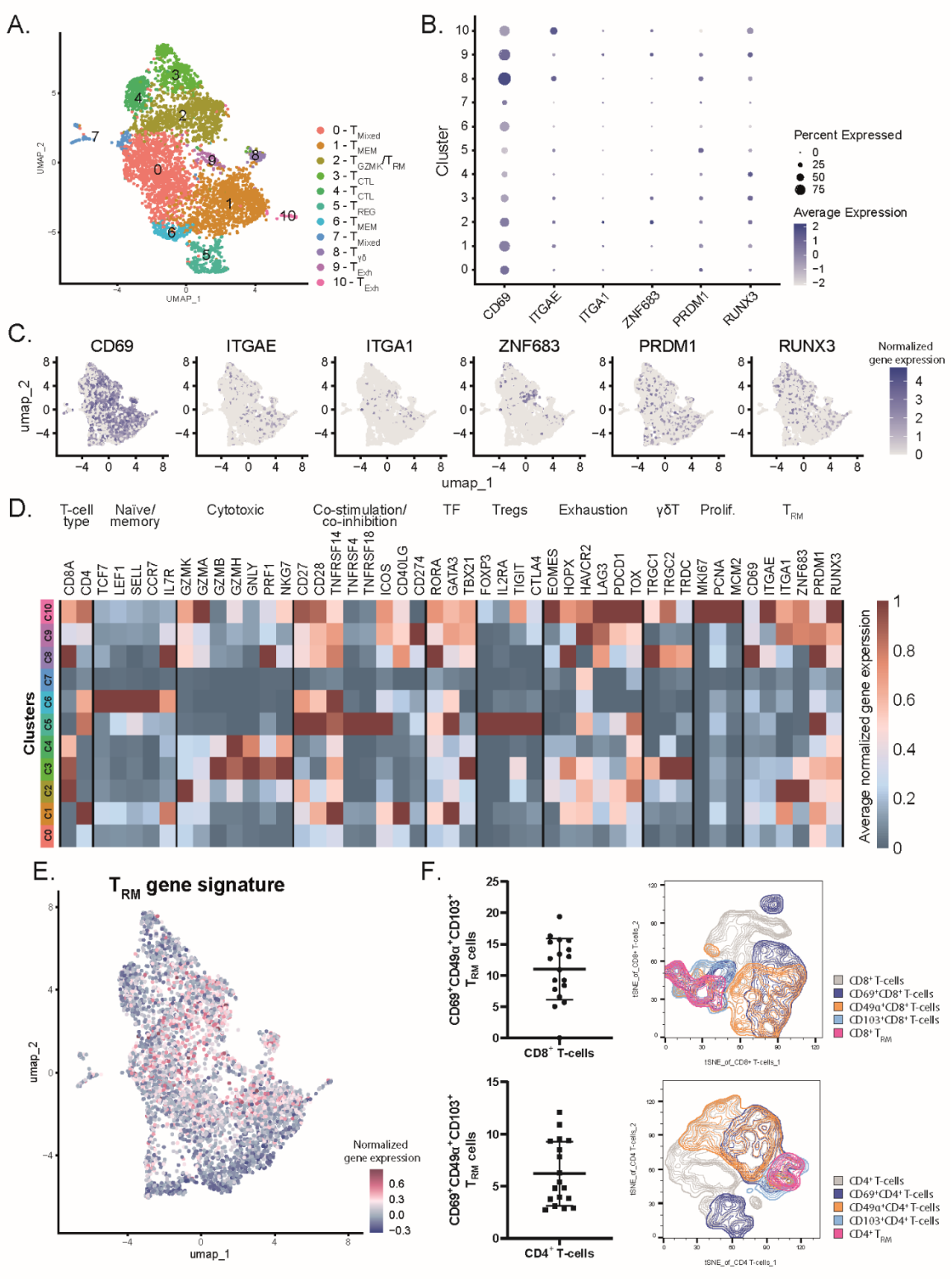

Figure 1. T_{RM} associated marker expression in human atherosclerotic lesions. A. UMAP representation of single cell RNA sequencing data of T-cells from human atherosclerotic lesions (n=4548) B. Dotplot visualizing average T_{RM} associated marker gene expression per cluster. C. Feature plot representation of T_{RM} marker expression. D. Heatmap displaying average expression of T cell function-associated genes per cluster. E. Projection of T_{RM} gene signature onto UMAP representation of plaque derived T-cells. F. Flow cytometry analysis of CD69, CD49α and CD103 expression by plaque derived CD4+ and CD8+ T-cells, demonstrating the percentage of CD69+CD49α+CD103+ co-expressing cells in a bar graph and tSNE representation.

RESULTS

Quantification of the proportion of T_{RM} in human atherosclerotic lesions.

Resident memory T-cells (T_{RM}) have been identified at the site of former inflammation in a large variety of tissues. Here, we interrogated T-cells from human atherosclerotic lesions on a single-cell level, to thoroughly evaluate the presence of T_{RM} cells in atherosclerosis. T_{RM} cells are notoriously heterogenic between tissues, making it challenging to identify T_{RM} cells in unexplored tissues by flowcytometry. Therefore, we used an in-house single-cell RNA sequencing (scRNAseq) dataset encompassing information on the transcriptome of three human atherosclerotic plaque samples, obtained via endarterectomy of the carotid artery, along with patient matched blood samples[6].

Subclustering of T-cells residing in the atherosclerosis lesion resulted in 11 clusters, including 2 mixed T-cell clusters (cluster 0 and 7), 1 regulatory cluster (cluster 5), 2 memory T-cell clusters (cluster 1 and 6), 2 exhausted T-cell clusters (cluster 9 and 10), 1 γδ T-cell cluster (cluster 8), 2 cytotoxic lymphocyte clusters (cluster 3 and 4) and 1 $GZMK^+$ T_{RM} -like cluster (cluster 2) (Figure 1A). In order to identify T_{RM} cells within the atherosclerotic lesions, we analyzed the expression of canonical T_{RM} marker, *CD69*, as well as markers strongly associated with a T_{RM} phenotype, such as *CD49A* and *integrin alpha E* (*ITGAE)* (encoding CD103), and transcription factors essential for the formation of T_{RM} cells, including *zinc finger protein 683* (*ZNF683)* (encoding Homolog of Blimp-1 in T-cells (HOBIT)), *PRDM1* (encoding B lymphocyte-induced maturation protein-1 (BLIMP-1)), and *RUNX3*). T_{RM} associated markers were mainly expressed by exhausted T-cell clusters 9 and 10, and by cytotoxic $GZMK^+$ cells from cluster 2 (Figure 1B, C and D). Projection of a T_{RM} gene signature, including "core" T_{RM} genes identified by Kumar et al. (2017) and T_{RM} associated transcription factors, onto the plaque derived T-cells identified cluster 0, 1, 2, 8 and 9 as clusters that potentially contain T_{RM} (Figure 1E). This T_{RM} gene signature was mainly expressed by T-cells from the atherosclerotic lesion, and to a minor extent by T-cells from circulation, confirming its specificity for tissue residing T-cells (Suppl. Figure 1). Moreover, co-expression of multiple T_{RM} markers, including CD69, CD49α, and CD103, was also confirmed on a protein level in human endarterectomy samples by flow cytometry (Figure 1F).

To more comprehensively evaluate how the phenotype of plaque derived T-cells relates to that of T_{RM} cells, T-cells with a canonical T_{RM} phenotype (expressing CD69, ITGAE and ZNF683) were selected from a previously published T_{RM} dataset, and integrated (Suppl. Figure 2)[14]. This T_{RM} dataset consisted of scRNAseq data of donor-derived T_{RM} cells extracted from intestinal transplant tissue 1 year after transplant using human leukocyte antigen (HLA) allele congenic cell tracking, ensuring the selection of long-lived T_{RM} cells. Reclustering of the curated dataset resulted in 10 distinct T-cell clusters, with the predefined T_{RM} cells predominately co-clustering with cells from cluster 3, demonstrating that a small proportion of plaque-residing T-cells exhibits a T_{RM}-like phenotype (approximately 4,6%) (Figure 2A-C). The plaque derived T-cells from cluster 3 mainly originated from cluster 2 in the original clustering (Figure 2E), a clusters that was already associated with T_{RM} marker expression.

To identify the expression profile of plaque derived T-cells from cluster 3, we excluded integrated T_{RM} cells from further analysis. T-cells from cluster 3 were characterized by relatively high expression of T_{RM} associated genes *CD69, ITGAE, ITGA1, ZNF683* and *RUNX3* (Figure 2D). Moreover, genes associated with T-cell activation and cytotoxicity, including *KLRK1* (NKG2D), *CCL5*, *MATK*, *KLRC4*, and *CTSW* (encoding cathepsin C), were amongst the top differentially expressed genes (Figure 2E), underlining the high cytolytic potential of the T_{RM}-like T-cells in the lesion.

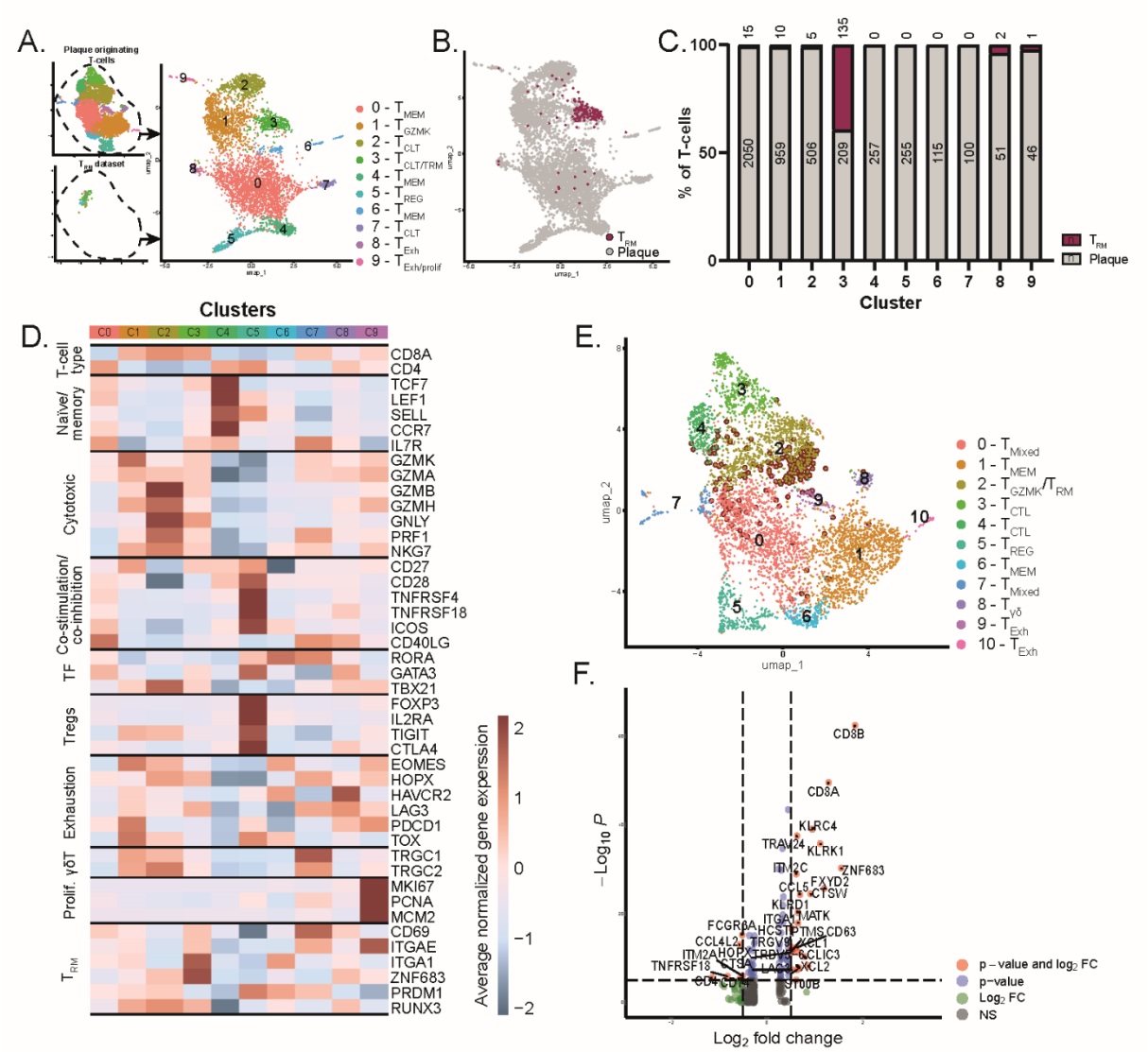

Figure 2. Predefined T_{RM} cells cluster together with plaque derived T-cells. A. UMAP representation after integration of (AI) plaque derived T-cells from the atherosclerosis scRNAseq dataset, and (AII) predefined T_{RM} cells. B. Projection of predefined T_{RM} cells on unsupervised T-cell clustering of the curated dataset. C. Percentage of integrated T_{RM} cells per cluster, with the number of integrated cells per cluster on top of each bar, and the number of plaque derived T-cells in the middle of each bar. D. Heatmap displaying average expression of T cell function-associated genes per cluster**.** E. UMAP representation of single-cell RNA sequencing data of T-cells from human atherosclerotic lesions (clustering before integration), highlighting plaque derived T-cells from cluster 3 (clustering after integration). Highlighted cells are indicated with a read halo. F. Volcano plot displaying significantly differentially expressed genes of plaque derived T-cells from cluster 3, compared to T-cells from all other clusters. Significantly differentially expressed genes were identified by Wilcoxon rank sum test, reaching statistical significance from $P < 10^{-6}$.

Phenotyping T_{RM} cells in the atherosclerotic environment.

As the scRNAseq analysis suggests the presence of a minor subset of T_{RM} in atherosclerotic lesions of patients, we next aimed to address their presence and role in the pathogenesis of atherosclerosis in mice. To corroborate the presence of T_{RM} in atherosclerotic lesions, a bone marrow transplant study was performed in *Rag1*$^{-/-}$*Ldlr*$^{-/-}$ mice, receiving bone marrow of Hobit reporter mice (Hobit^{tdTomato}). In Hobit^{tdTomato} mice the *Znf683* promoter of one allele was

inserted with the *tdTomato* gene, encoding a red fluorescent protein[19]. After reconstitution of the bone marrow, mice were fed a Western-type diet for 10 weeks to induce atherosclerosis.

To address whether the Hobit reporter allowed detection of T_{RM} after bone marrow transplantation, we first examined T_{RM} in the liver which naturally contains these cells. We observed that the percentage of tdTomato$^+$ T-cells in the liver varied from 2.5 - 8% for CD4$^+$ T-cells and between 7 - 26% for CD8$^+$ T-cells, which is consistent with previously reported numbers of T_{RM} in livers of naïve mice (Figure 3A, S3A-B)[20]. TdTomato$^+$ CD4$^+$ and CD8$^+$ T-cells from the liver almost uniformly expressed CD69 whereas tdTomato$^-$ T-cells harbored a limited number of CD69 positive cells. Moreover, tdTomato$^+$ CD4$^+$ and CD8$^+$ T-cells expressed significantly elevated levels of CD49α, compared to their tdTomato$^-$ counterparts. The increased expression of CD69 and CD49α suggests that tdTomato$^+$ T-cells indeed positively identify as T_{RM} cells.

Next we analyzed the number of T_{RM} in the aortic arch, a primary site of atherosclerotic lesion development. The proportion of tdTomato-expressing T-cells in the atherosclerotic lesion ranged from 0-6% for CD4$^+$ T-cells and between 1-7% for CD8$^+$ T-cells (Figure 3B, S3C-D). The proportion of CD69$^+$ cells was significantly increased in the tdTomato$^+$ T-cells compared to the tdTomato$^-$ T-cells. However, CD69 was not exclusively expressed by tdTomato$^+$ T-cells in the aorta, in line with previous reports suggesting that CD69 is upregulated in lesion-derived T-cells as a response to antigen-specific interactions. Hence, CD69 cannot be considered as a standalone marker for identifying T_{RM} cells in the lesion.

Additional markers that were evaluated as potential T_{RM} markers in the lesion were CD49α and CD103. TdTomato$^+$ T-cells in the lesion trended towards an upregulated expression of CD49α. Moreover, almost all CD49α$^+$ cells also co-expressed CD69 (Suppl. Figure 3E-F). Integrin CD103, on the other hand, is a canonical T_{RM} marker for T_{RM} cells in epithelial and mucosal tissues and is differentially expressed by T_{RM} cells in the lesion. Hobit$^+$ CD4$^+$ T-cells expressed elevated CD103 levels compared to their Hobit$^-$ counterparts. Although CD103 was highly expressed by CD8$^+$ T-cells in the atherosclerotic lesion, it appeared to be mainly expressed by tdTomato$^-$ CD8$^+$ T-cells as opposed to tdTomato$^+$ CD8$^+$ T-cells, demonstrating CD103 alone is not a suitable marker for identifying CD8$^+$ T_{RM} cells in atherosclerosis. Co-expression of CD103 together with CD69, however, was almost exclusive to tdTomato$^+$ T-cells, compared to tdTomato$^-$ cells (Suppl. Figure 3E-F). Taken together, tracking of T_{RM} cells revealed CD69 and CD49α as markers characteristic for T_{RM} in the atherosclerotic lesion.

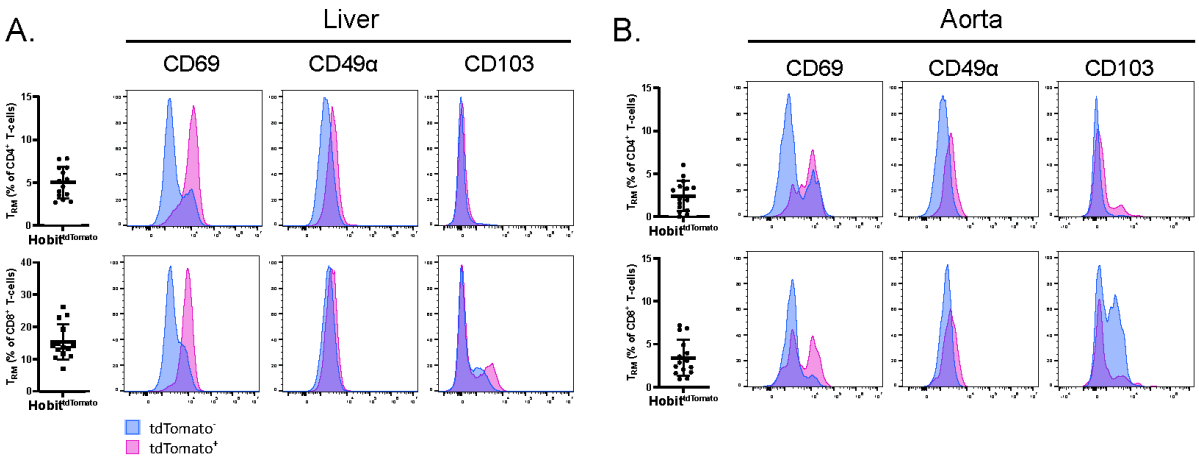

Figure 3. Lesion-derived T_{RM} cells are characterized by elevated expression of CD69 and CD49α. A. The percentage of Hobit-expressing tdTomato$^+$ CD4$^+$ and CD8$^+$ T-cells and the expression of CD69, CD49α, and CD103 by tdTomato$^+$ (pink) and tdTomato$^-$ (blue) in the liver, B. and in the aorta.

T_{RM} cells constitute only a minor population in atherosclerotic lesions.

Next, we set out to discover the role of T_{RM} cells in the pathogenesis of atherosclerosis. B lymphocyte-induced maturation protein-1 (Blimp-1) and Homolog of Blimp-1 in T-cells (Hobit) are central regulators of the conversion of T-cells to a tissue-resident phenotype in both classical, as well as innate lymphocytes[20]. To investigate the function of T_{RM} in atherosclerosis, we performed a bone marrow transplant experiment with bone marrow originating from Hobit$^{KO/CRE}$Blimp-1$^{flox/flox}$ mice (Hobit$^{CRE/tdTomato}$ x Blimp-1$^{flox/flox}$ mice), or wildtype mice (C57BL/6 mice) transferred to *Rag1$^{-/-}$Ldlr$^{-/-}$* mice (Suppl. Figure 4A). By knocking out Hobit, and conditionally disrupting Blimp-1 in cells with an active *Znf683* promoter, the formation of T_{RM} cells can be severely reduced[18,20]. Hobit$^{CRE/tdTomato}$ x Blimp-1$^{flox/flox}$ mice exhibit a significantly reduced number of T_{RM}[18]. Moreover, the tdTomato$^+$ T_{RM} progenitor cells that remained expressed reduced levels of retention molecule CD69, as well as increased levels of tissue egress markers S1PR1 and CCR7, demonstrating that these cells are not capable of obtaining a mature T_{RM} phenotype. After recovery of the bone marrow transplant, mice were fed a Western-type diet (WTD) for 10 weeks to induce atherosclerosis formation. Throughout the experiment, mouse weights and cholesterol levels were similar between groups (Suppl. Figure 4A-C). At the end of the experiment the hampered formation of T_{RM} cells was confirmed in the liver by evaluating CD69$^+$ T-cell counts (Suppl. Figure 5).

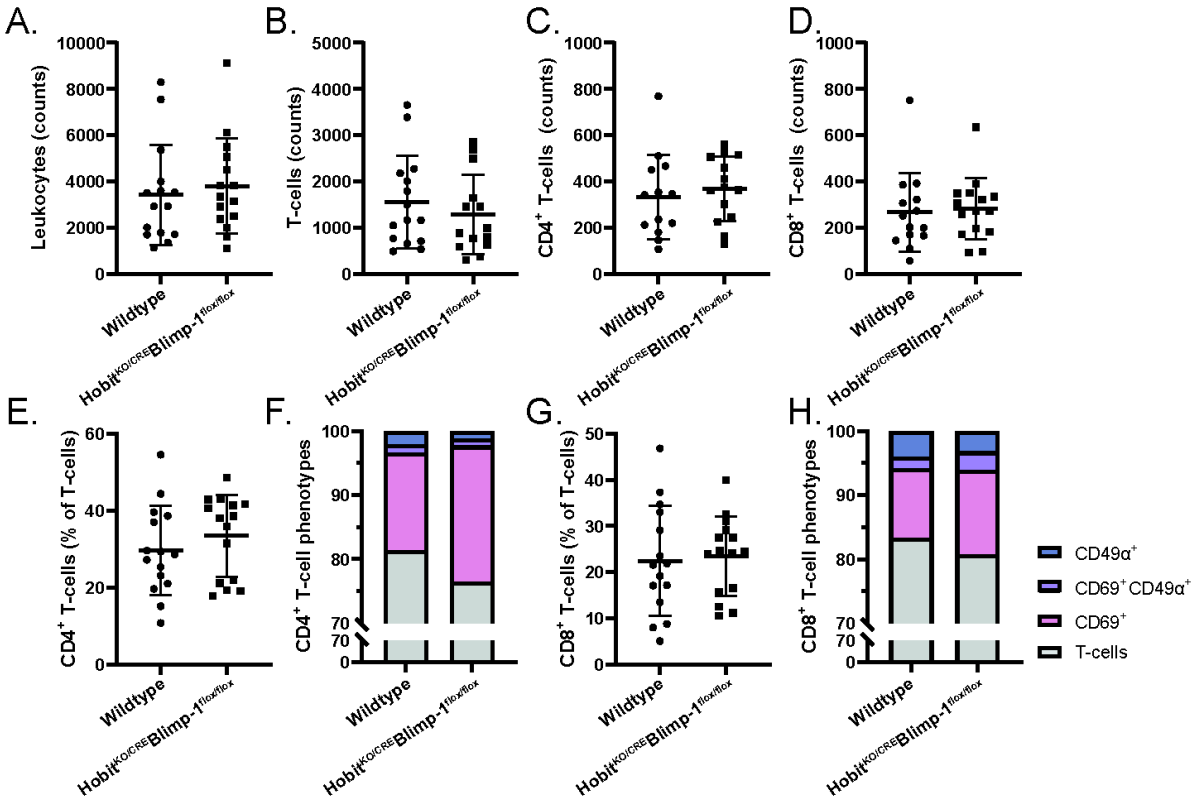

Figure 4. Reduction of T_{RM} cells does not affect leukocyte numbers or T-cell populations in the atherosclerotic lesion. A. Absolute leukocyte (CD45), B. T-cell (Thy1.2), C. CD4$^+$ T-cell (Thy1.2$^+$CD4$^+$), and D. CD8$^+$ T-cell (Thy1.2$^+$CD8$^+$) numbers in the aorta. E. Fraction of CD4$^+$ T-cells (as a percentage of total T-cells). F. Proportion of CD69$^+$, CD49α$^+$ and CD69$^+$CD49α$^+$ expressing CD4$^+$ T-cells (as a percentage of total CD4$^+$ T-cells). E. Fraction of CD8$^+$ T-cells (as a percentage of total T-cells). F. Proportion of CD69$^+$, CD49α$^+$ and CD69$^+$CD49α$^+$ expressing CD8$^+$ T-cells (as a percentage of total CD8$^+$ T-cells). Plot contain individual data points with mean ± SD. Significance was determined by unpaired t-test. Outliers were removed after a ROUT test.

The blocked T_{RM} formation resulted in some variations in circulating immune cell levels, while leukocyte populations in secondary lymphoid organs remained unaffected (Suppl. Figure 4D-E). Given that Hobit and Blimp-1 are important for the differentiation of innate lymphoid cells as well, the distribution of natural killer (NK) cells and natural killer T (NKT) cells in the liver was evaluated[20,21]. The fraction of NK and NKT cells, which are low due to the bone marrow transplantation, were significantly reduced in the livers of Hobit$^{KO/CRE}$Blimp-1$^{flox/flox}$ mice (Suppl. Figure 4F). Also, the cytolytic capacity of NK-cells was affected by the Hobit/Blimp-1 knockout, apparent from a significantly reduced GZMB$^+$ NK-cell population.

In the lesion however, general leukocyte levels and T-cell numbers were not affected by the knockdown of T_{RM} cells (Figure 4A-E, G). Interestingly, we also did not observe changes in the CD69$^+$ or CD49α$^+$ T-cell populations, and only a modest decrease in the percentage of CD69$^+$CD49α$^+$ double positive CD8$^+$ T-cells (Figure 4F, H, S6). The marginal changes in T_{RM} marker expressing T-cell populations underlines that T_{RM} only encompass a minor population in the atherosclerotic lesion.

T_{RM} cells associate with reduced macrophage content and increased collagen deposition in atherosclerotic lesions.

To verify the effects of the Hobit/Blimp-1 conditional double knockout on the progression of atherosclerosis, plaque size and composition was assessed in the aortic root lesions of the heart by histological analysis. Neutral lipid-staining of the lesions by Oil-Red-O demonstrated similar absolute plaque sizes, with an approximate plaque size of 400.000μm^2, and comparable vascular occlusion, of approximately 40%, between groups (Figure 5A). Although plaque size was not altered by the lack of T_{RM}, plaque composition was affected in the Hobit$^{KO/CRE}$Blimp-1$^{flox/flox}$ group. The macrophage positive stained area as a relative to plaque size was significantly increased in Hobit$^{KO/CRE}$Blimp-1$^{flox/flox}$ mice, with a 1.33-fold increase compared to the wildtype control (Figure 5B). Interestingly, the increased macrophage content did not translate to increased necrotic core sizes, evaluated by Masson trichrome staining (Figure 5C). Collagen content, on the other hand, trended towards a reduction in Hobit$^{KO/CRE}$Blimp-1$^{flox/flox}$ mice.

DISCUSSION

Tissue-resident memory T-cells are a relatively newly discovered T-cell subset, that forms the first line of defense against secondary infections. Despite the growing body of knowledge, the precise role of this specialized T-cell subset in chronic inflammatory diseases remains largely elusive[22,23]. This study contributes valuable insights on the presence, phenotype and functionality of T_{RM} in both human and mouse atherosclerotic lesions. We demonstrated that T_{RM} constitute a minor fraction of the lymphocyte population in the atherosclerotic lesion, and that mice in which the formation of T_{RM} was hindered exhibit increased lesion stability.

In human atherosclerotic lesions, we identified a minor population of T_{RM}-like cells that expressed elevated levels of T_{RM} associated genes, and co-clustered with predefined T_{RM} cells for intestinal epithelium. Although the phenotype of these predefined T_{RM} cells might be effected by other microenvironmental circumstances (different tissue, disease, and medical background of the patient), they specifically clustered together with the plaque-derived T cells that expressed a T_{RM}-like phenotype in the unintegrated analysis, suggesting a common core T_{RM} signature for T_{RM} derived from different tissues[15]. The T_{RM}-like cells in the atherosclerotic lesion were characterized by the expression of CD69, ITGA1, ITGAE, on both transcriptional and translational level, and a transcription factor profile associated with the T_{RM} phenotype.

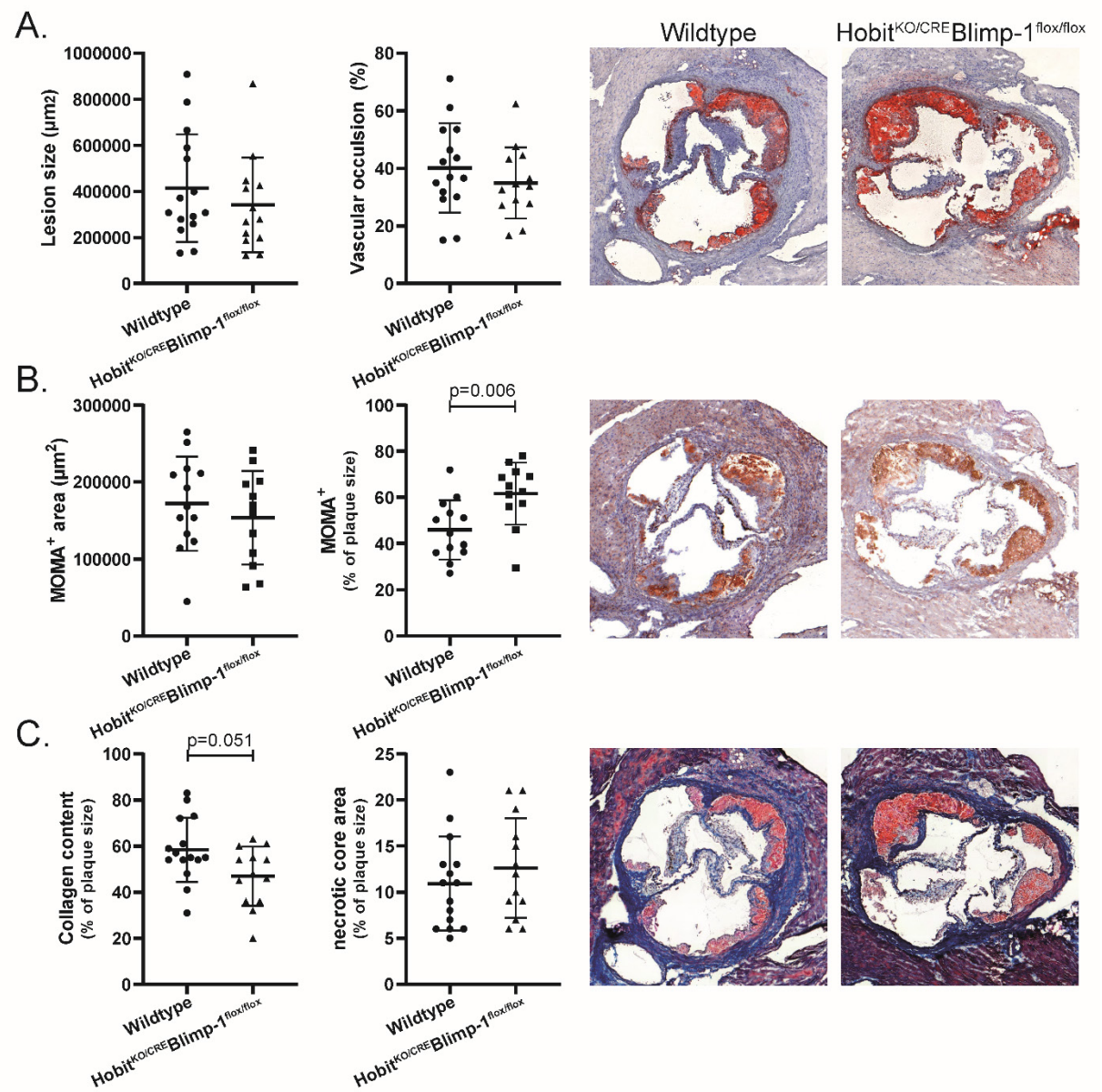

Figure 5. Hindered T_{RM} formation results in a relative increase in intralesional macrophages and reduction in collagen content. (A) Quantification of lesion size and vascular occlusion in the trivalve area determined by Oil-red O staining and representative pictures of the wildtype and Hobit$^{KO/CRE}$Blimp-1$^{flox/flox}$ groups (B) Quantification of absolute and relative monocyte/macrophage content in the plaque by MOMA staining and representative pictures of the lesions. (C) Quantification of relative necrotic core area and relative collagen content in the lesions after Masson's Trichrome staining and representative pictures of the lesions. Plot contain individual data points with mean ± SD. Significance was determined by unpaired t-test. Outliers were removed after a ROUT test.

The upregulated expression of CD69 and CD49α was corroborated in mice. Although human T_{RM} cells might be characterized by the expression of CD103, as shown here and by others[2], this marker was inconsistently expressed by Hobit-expressing $CD4^+$ and $CD8^+$ T-cells in mouse atherosclerotic lesions. Various studies demonstrated species-specific differences in T_{RM} phenotype within the same tissue[24]. Moreover, T_{RM} located in non-epithelial/mucosal tissues often refrain from expressing CD103, as its ligand, E-cadherin, is not expressed there[25]. Conversely, a large proportion of Hobit$^-$ $CD8^+$ T-cells did express CD103 in the atherosclerotic

lesion. CD103 expression is enhanced by exposure to TGFβ, a cytokine expressed in atherosclerotic lesions and associated with protection against plaque rupture[26,27].

Like the expression of CD103, the expression of CD69 was also not confined to T_{RM} cells. A substantial population of approximately 20% of the $CD4^+$ and $CD8^+$ T-cells expressed CD69 in mouse atherosclerotic lesions. However, on average only 2.4% of the T-cells expressed Hobit, suggesting that the majority of CD69 positive cells did not identify as T_{RM}. Lesional T-cells have been reported to express an activated phenotype and display signs clonal expansion and tissue enrichment, implying recent activation through TCR specific interactions[6,28]. Hence, it seems that merely a fraction of CD69-expressing cells in the lesion possess a T_{RM} phenotype, while for the remaining cells potentially upregulated CD69 as a response to antigen recognition.

One limitation of our approach is that by identifying T_{RM} cells based on Hobit expression we may have underestimated the T_{RM} population. Although Hobit is exclusively expressed by T_{RM}, and not by other antigen experienced T-cell populations, this marker might be downregulated over time by some T_{RM} cells, rendering identification in this study setup impossible[18,29]. Nonetheless, the knockdown of T_{RM} cells did not impact the proportion of T-cells in the lesion, nor the percentage of CD69 expressing T-cells, indicating that the T_{RM} population is indeed a very small fraction of the T-cell population.

In spite of their modest representation, we did observe a significantly reduced plaque stability and increased macrophage content when T_{RM} cells were significantly reduced. However, these effects might not be fully attributable to the lack of T_{RM} cells, as we also observed changes in circulating leukocyte levels and a significant reduction in innate lymphocyte populations. Although NK- and NKT-cells have been detected inside atherosclerotic lesions, their function in atherosclerosis remains controversial. A recent study on the function of NK-cells in atherosclerosis concluded that depletion of NK-cells does not affect the progression of atherosclerosis[30]. In addition, most reports focusing on the function of NKT-cells in atherosclerosis describe an aggravating effect of NKT-cells in atherosclerosis, which does not explain the effects observed in this study[31].

Moreover, similar protective effects were observed when all $CD8^+$ T-cells – including all cytotoxic T-cells – were depleted from advanced atherosclerotic lesions[32], or, when $CD4^+$ T-cell numbers were strongly reduced and their interaction with MHCII was negated[33]. In line with previous reports focusing on the phenotype of T_{RM} cells, scRNAseq of human atherosclerotic lesions revealed that T_{RM}-like cells in the lesion expressed high levels of granzymes and other cytotoxicity associated molecules[34]. These cytolytic T-cells might control intralesional macrophage content by specifically targeting macrophages. Moreover, antigen-specific CD8+ T-cells have also been shown to exert atheroprotective effects[35,36]. The observed changes in collagen content might be a result of the relatively increased macrophage population, as macrophages express a variety of matrix degrading enzymes, like metalloproteinases, that contribute to the breakdown of the collagen in the fibrous cap[37,38].

Interestingly, in most immune disorders, like rheumatoid arthritis, inflammatory bowel disease, and psoriasis, T_{RM} are associated with disease acceleration. Yet, unlike atherosclerosis, these diseases are characterized by a relapsing-remitting course, and T_{RM} cells have been implicated to contribute to these recurring disease flares[10,11,39]. Atherosclerosis, on the other hand, is an ongoing chronic inflammatory disease characterized by constant immune cell infiltration, persistent chemokine and cytokine production, and continuous antigen presentation[6]. The chronic nature of the disease might explain the limited formation of T_{RM} cell in the lesion. Although some reports argue persistent low-gradient antigen presentation induces memory

inflation and increase T_{RM} populations[40], others showed compromised T_{RM} formation after chronic viral infection, compared to acute infection[41].

In conclusion, this study provides valuable insights into the presence, phenotype and function of T_{RM} cells in human and mouse atherosclerotic lesions. We demonstrate that intralesional T_{RM} cells are characterized by the expression of CD69 and CD49α and that although these T_{RM} cells only constitute a minor T-cell population within the lesion, their presence associated with reduced atherosclerotic burden by decreasing the amount of intralesional macrophages and enhancing lesion stability.

FUNDING

This work was supported by The Dutch Heart Foundation (CVON2017-20: GENIUS II, awarded to JK), European Research Area Network on Cardiovascular Diseases (ERA-CVD, 2018T092, awarded to BS),

DISCLOSURES

The authors have no conflicts of interest.

SUPPLEMENTARY DOCUMENTS

Suppl. Figure 1-10

Table S1

REFERENCES

1. Depuydt MAC, Prange KHM, Slenders L, Örd T, Elbersen D, Boltjes A, De Jager SCA, Asselbergs FW, De Borst GJ, Aavik E, et al. Microanatomy of the Human Atherosclerotic Plaque by Single-Cell Transcriptomics. *Circ. Res.* [Internet]. 2020 [cited 2020 Dec 16];127:1437–1455. Available from: https://www.ahajournals.org/doi/suppl/10.1161/CIRCRESAHA.120.316770.
2. Fernandez DM, Rahman AH, Fernandez NF, Chudnovskiy A, Amir E ad D, Amadori L, Khan NS, Wong CK, Shamailova R, Hill CA, et al. Single-cell immune landscape of human atherosclerotic plaques. *Nat. Med.* 2019;25:1576–1588.
3. Winkels H, Ehinger E, Vassallo M, Buscher K, Dinh HQ, Kobiyama K, Hamers AAJ, Cochain C, Vafadarnejad E, Saliba AE, et al. Atlas of the immune cell repertoire in mouse atherosclerosis defined by single-cell RNA-sequencing and mass cytometry. *Circ. Res.* 2018;
4. Smit V, de Mol J, Schaftenaar F, Depuydt M, Postel R, Smeets D, Verheijen F, Bogers L, van Duijn J, Verwilligen R, et al. Single-cell profiling reveals age-associated immunity in atherosclerosis. *Cardiovasc. Res.* 2023;
5. Saigusa R, Winkels H, Ley K. T cell subsets and functions in atherosclerosis. *Nat. Rev. Cardiol. 2020 177* [Internet]. 2020 [cited 2023 Aug 29];17:387–401. Available from: https://www.nature.com/articles/s41569-020-0352-5
6. Depuydt MAC, Schaftenaar FH, Prange KHM, Boltjes A, Hemme E, Delfos L, De Mol J, De Jong MJM, Kleijn MNAB, Peeters JAHM, et al. Single-cell T cell receptor sequencing of paired human atherosclerotic plaques and blood reveals autoimmune-like features of expanded effector T cells. [cited 2023 Feb 9];Available from: https://doi.org/10.1038/s44161-022-00208-4
7. Urban SL, Berg LJ, Welsh RM. Type 1 interferon licenses naïve CD8 T cells to mediate anti-viral cytotoxicity. *Virology*. 2016;493:52–59.
8. Cibrián D, Sánchez-Madrid F. CD69: from activation marker to metabolic gatekeeper. *Eur. J. Immunol.* [Internet]. 2017 [cited 2022 Sep 16];47:946–953. Available from: https://pubmed.ncbi.nlm.nih.gov/28475283/
9. Zhang Z, Qiu S, Zhang X, Chen W. Optimized DNA electroporation for primary human T cell engineering. *BMC Biotechnol.* [Internet]. 2018 [cited 2020 May 20];18:4. Available from: https://bmcbiotechnol.biomedcentral.com/articles/10.1186/s12896-018-0419-0
10. Zundler S, Becker E, Spocinska M, Slawik M, Parga-Vidal L, Stark R, Wiendl M, Atreya R, Rath T, Leppkes M, et al. Hobit- and Blimp-1-driven CD4+ tissue-resident memory T cells control chronic intestinal inflammation. *Nat. Immunol.* 2019;
11. Chang MH, Levescot A, Nelson-Maney N, Blaustein RB, Winden KD, Morris A, Wactor A, Balu S, Grieshaber-Bouyer R, Wei K, et al. Arthritis flares mediated by tissue-resident memory T cells in the joint. *Cell Rep.* 2021;
12. Wang Z, Zhang X, Lu S, Zhang C, Ma Z, Su R, Li Y, Sun T, Li Y, Hong M, et al. Pairing of single-cell RNA analysis and T cell antigen receptor profiling indicates breakdown of T cell tolerance checkpoints in atherosclerosis. *Nat. Cardiovasc. Res.* [Internet]. 2023 [cited 2023 Nov 6];2:290–306. Available from: https://doi.org/10.1038/s44161-023-00218-w
13. Winkels H, Wolf D. Heterogeneity of T Cells in Atherosclerosis Defined by Single-Cell RNA-Sequencing and Cytometry by Time of Flight. *Arterioscler. Thromb. Vasc. Biol.* [Internet]. 2021 [cited 2022 Feb 13];41:549–563. Available from: www.ahajournals.org/atvb/atvb-focus
14. FitzPatrick MEB, Provine NM, Garner LC, Powell K, Amini A, Irwin SL, Ferry H, Ambrose T, Friend P, Vrakas G, et al. Human intestinal tissue-resident memory T cells comprise transcriptionally and functionally distinct subsets. *Cell Rep.* [Internet]. 2021 [cited 2023 Aug 3];34. Available from: /pmc/articles/PMC7816164/
15. Kumar B V., Ma W, Miron M, Granot T, Guyer RS, Carpenter DJ, Senda T, Sun X, Ho SH, Lerner H, et al. Human Tissue-Resident Memory T Cells Are Defined by Core Transcriptional and Functional Signatures in Lymphoid and Mucosal Sites. *Cell Rep.* 2017;20:2921–2934.
16. Behr FM, Parga-Vidal L, Kragten NAM, van Dam TJP, Wesselink TH, Sheridan BS, Arens R, van Lier RAW, Stark R, van Gisbergen KPJM. Tissue-resident memory CD8+ T cells shape local and systemic secondary T cell responses. *Nat. Immunol. 2020 219* [Internet]. 2020 [cited 2023 Sep 1];21:1070–1081. Available from: https://www.nature.com/articles/s41590-020-0723-4
17. Van Gisbergen KPJM, Kragten NAM, Hertoghs KML, Wensveen FM, Jonjic S, Hamann J, Nolte MA, Van Lier RAW. Mouse Hobit is a homolog of the transcriptional repressor Blimp-1 that regulates NKT cell effector differentiation. *Nat. Immunol. 2012 139* [Internet]. 2012 [cited 2023 Sep 11];13:864–871. Available from: https://www.nature.com/articles/ni.2393
18. Parga-Vidal L, Taggenbrock RLRE, Beumer-Chuwonpad A, Aglmous H, Kragten NAM, Behr FM, Bovens AA, van Lier RAW, Stark R, van Gisbergen KPJM. Hobit and Blimp-1 regulate TRM abundance

after LCMV infection by suppressing tissue exit pathways of TRMprecursors. *Eur. J. Immunol.* [Internet]. 2022 [cited 2023 Aug 29];52:1095. Available from: /pmc/articles/PMC9545210/

19. Shaner NC, Campbell RE, Steinbach PA, Giepmans BNG, Palmer AE, Tsien RY. Improved monomeric red, orange and yellow fluorescent proteins derived from Discosoma sp. red fluorescent protein. *Nat. Biotechnol. 2004 2212* [Internet]. 2004 [cited 2023 Aug 28];22:1567–1572. Available from: https://www.nature.com/articles/nbt1037
20. Mackay LK, Minnich M, Kragten NAM, Liao Y, Nota B, Seillet C, Zaid A, Man K, Preston S, Freestone D, et al. Hobit and Blimp1 instruct a universal transcriptional program of tissue residency in lymphocytes. *Science (80-.).* 2016;352:459–463.
21. Kragten NA, Taggenbrock RL, Parga Vidal L, van Lier RA, Stark R, van Gisbergen KP. Hobit and Blimp-1 instruct the differentiation of iNKT cells into resident-phenotype lymphocytes after lineage commitment. *Eur. J. Immunol.* [Internet]. 2022 [cited 2022 Jan 10];Available from: https://onlinelibrary.wiley.com/doi/10.1002/eji.202149360
22. Wu H, Liao W, Li Q, Long H, Yin H, Zhao M, Chan V, Lau CS, Lu Q. Pathogenic role of tissue-resident memory T cells in autoimmune diseases. Autoimmun. Rev. 2018;
23. Samat AAK, van der Geest J, Vastert SJ, van Loosdregt J, van Wijk F. Tissue–Resident Memory T Cells in Chronic Inflammation—Local Cells with Systemic Effects? *Cells* [Internet]. 2021 [cited 2023 Sep 4];10:1–19. Available from: /pmc/articles/PMC7920248/
24. Szabo PA, Miron M, Farber DL. Location, location, location: Tissue resident memory T cells in mice and humans. *Sci. Immunol.* [Internet]. 2019 [cited 2023 Jul 4];4:9673. Available from: https://www.science.org
25. Behr FM, Chuwonpad A, Stark R, van Gisbergen KPJM. Armed and Ready: Transcriptional Regulation of Tissue-Resident Memory CD8 T Cells. Front. Immunol. 2018;9:1770.
26. Edsfeldt A, Singh P, Matthes F, Tengryd C, Cavalera M, Bengtsson E, Dunér P, Volkov P, Karadimou G, Gisterå A, et al. Transforming growth factor-β2 is associated with atherosclerotic plaque stability and lower risk for cardiovascular events. *Cardiovasc. Res.* [Internet]. 2023 [cited 2023 Sep 14];119:2061–2073. Available from: https://dx.doi.org/10.1093/cvr/cvad079
27. El-Asady R, Yuan R, Liu K, Wang D, Gress RE, Lucas PJ, Drachenberg CB, Hadley GA. TGF-β–dependent CD103 expression by CD8+ T cells promotes selective destruction of the host intestinal epithelium during graft-versus-host disease. *J. Exp. Med.* [Internet]. 2005 [cited 2023 Sep 14];201:1647. Available from: /pmc/articles/PMC2212926/
28. Chowdhury RR, D'Addabbo J, Huang X, Veizades S, Sasagawa K, Louis DM, Cheng P, Sokol J, Jensen A, Tso A, et al. Human Coronary Plaque T Cells Are Clonal and Cross-React to Virus and Self. *Circ. Res.* [Internet]. 2022 [cited 2022 Sep 2];130:1510–1530. Available from: http://www.ncbi.nlm.nih.gov/pubmed/35430876
29. Behr FM, Parga-Vidal L, Kragten NAM, van Dam TJP, Wesselink TH, Sheridan BS, Arens R, van Lier RAW, Stark R, van Gisbergen KPJM. Tissue-resident memory CD8+ T cells shape local and systemic secondary T cell responses. *Nat. Immunol. 2020 219* [Internet]. 2020 [cited 2024 Jan 8];21:1070–1081. Available from: https://www.nature.com/articles/s41590-020-0723-4
30. Nour-Eldine W, Joffre J, Zibara K, Esposito B, Giraud A, Zeboudj L, Vilar J, Terada M, Bruneval P, Vivier E, et al. Genetic Depletion or Hyperresponsiveness of Natural Killer Cells Do Not Affect Atherosclerosis Development. *Circ. Res.* [Internet]. 2018 [cited 2023 Sep 4];122:47–57. Available from: https://pubmed.ncbi.nlm.nih.gov/29046274/
31. Chakrabarti R, Duddu S, Tiwari A, Naidu KT, Sharma P, Chakravorty N, Shukla PC. Natural Killer T cells and the invariant subset promote atherosclerosis: A meta-analysis. *Life Sci.* 2023;321:121620.
32. Van Duijn J, Kritikou E, Benne N, Van Der Heijden T, Van Puijvelde GH, Kröner MJ, Schaftenaar FH, Foks AC, Wezel A, Smeets H, et al. CD8+ T-cells contribute to lesion stabilization in advanced atherosclerosis by limiting macrophage content and CD4+ T-cell responses. *Cardiovasc. Res.* 2019;115:729–738.
33. Wigren M, Rattik S, Yao Mattisson I, Tomas L, Grönberg C, Söderberg I, Alm R, Sundius L, Ljungcrantz I, Björkbacka H, et al. Lack of Ability to Present Antigens on Major Histocompatibility Complex Class II Molecules Aggravates Atherosclerosis in ApoE-/- Mice. *Circulation* [Internet]. 2019 [cited 2021 May 26];139:2554–2566. Available from: https://pubmed.ncbi.nlm.nih.gov/31136220/
34. Cheuk S, Schlums H, Gallais Sérézal I, Martini E, Chiang SC, Marquardt N, Gibbs A, Detlofsson E, Introini A, Forkel M, et al. CD49a Expression Defines Tissue-Resident CD8+ T Cells Poised for Cytotoxic Function in Human Skin. *Immunity* [Internet]. 2017 [cited 2023 Nov 7];46:287. Available from: /pmc/articles/PMC5337619/
35. Chyu KY, Zhao X, Dimayuga PC, Zhou J, Li X, Yano J, Lio WM, Chan LF, Kirzner J, Trinidad P, et al. CD8 + T cells mediate the athero-protective effect of immunization with an ApoB-100 peptide. *PLoS One*. 2012;7.
36. Dimayuga PC, Zhao X, Yano J, Lio WM, Zhou J, Mihailovic PM, Cercek B, Shah PK, Chyu KY.

Identification of apoB-100 Peptide-Specific CD8+ T Cells in Atherosclerosis. *J. Am. Hear. Assoc. Cardiovasc. Cerebrovasc. Dis.* [Internet]. 2017 [cited 2022 Oct 28];6. Available from: /pmc/articles/PMC5586274/

37. Libby P, Geng YJ, Aikawa M, Schoenbeck U, Mach F, Clinton SK, Sukhova GK, Lee RT. Macrophages and atherosclerotic plaque stability. *Curr. Opin. Lipidol.* [Internet]. 1996 [cited 2023 Nov 7];7:330–335. Available from: https://pubmed.ncbi.nlm.nih.gov/8937525/
38. Newby AC. Metalloproteinase production from macrophages - a perfect storm leading to atherosclerotic plaque rupture and myocardial infarction. *Exp. Physiol.* [Internet]. 2016 [cited 2023 Nov 7];101:1327–1337. Available from: https://pubmed.ncbi.nlm.nih.gov/26969796/
39. Chen L, Shen Z. Tissue-resident memory T cells and their biological characteristics in the recurrence of inflammatory skin disorders. Cell. Mol. Immunol. 2020;
40. Uddbäck I, Cartwright EK, Schøller AS, Wein AN, Hayward SL, Lobby J, Takamura S, Thomsen AR, Kohlmeier JE, Christensen JP. Long-term maintenance of lung resident memory T cells is mediated by persistent antigen. *Mucosal Immunol.* [Internet]. 2021 [cited 2023 Sep 14];14:92. Available from: /pmc/articles/PMC7726002/
41. Casey KA, Fraser KA, Schenkel JM, Moran A, Abt MC, Beura LK, Lucas PJ, Artis D, Wherry EJ, Hogquist K, et al. Antigen-Independent Differentiation and Maintenance of Effector-like Resident Memory T Cells in Tissues. *J. Immunol.* 2012;188:4866–4875.

SUPPLEMENTARY FIGURES

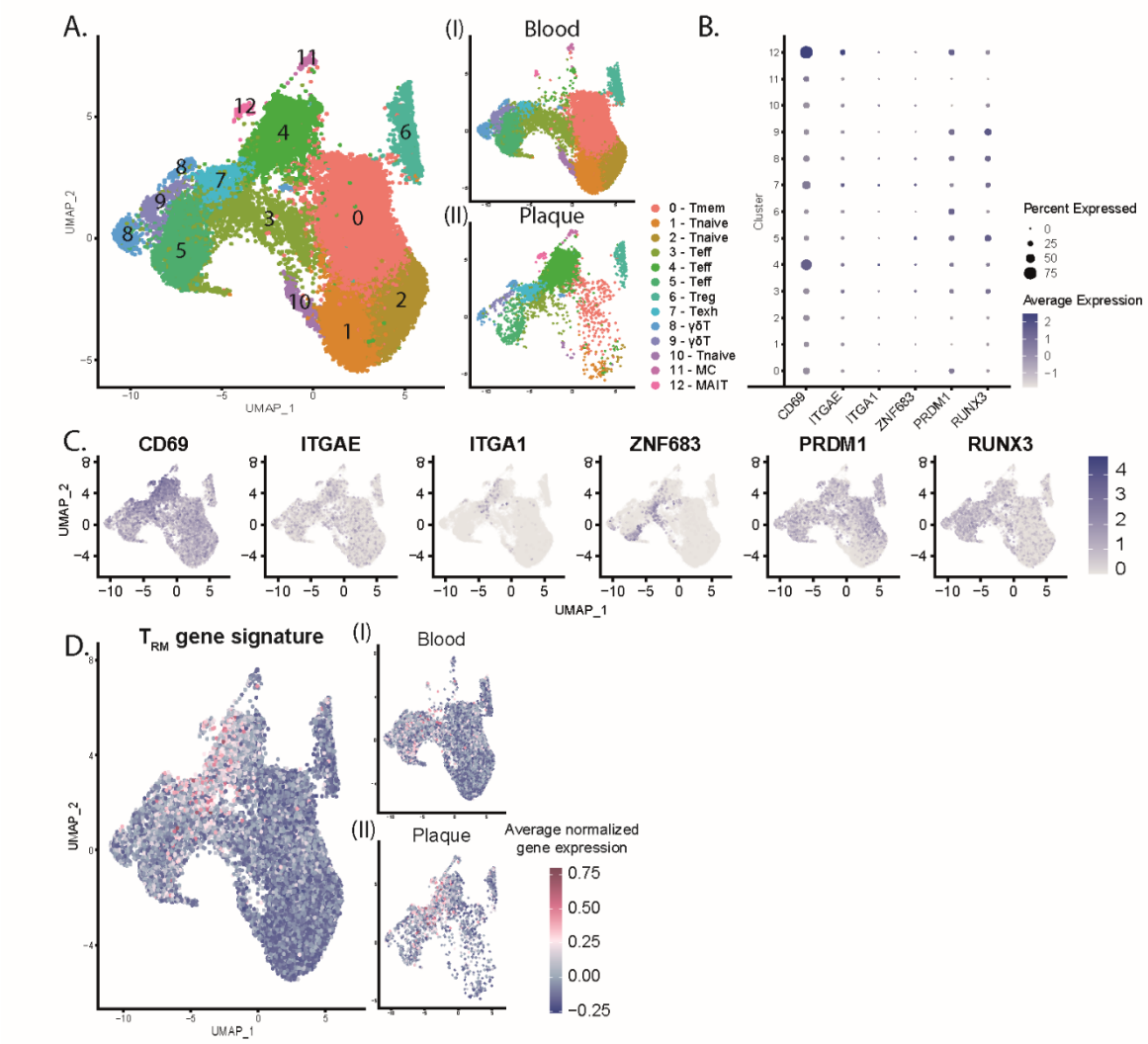

Supplemental figure 1. T_{RM} associated marker expression in human atherosclerotic lesions. A. UMAP representation of single cell RNA sequencing data of T-cells from human atherosclerotic lesions and patient matched blood samples (n=24443), subdivided in blood (AI) and plaque (AII). B. Dotplot visualization of the average expression of T_{RM} markers per cluster. C. Featureplot representation of T_{RM} marker expression. D. Projection of T_{RM} gene signature onto UMAP representation, subdivided in blood (DI) and plaque (DII).

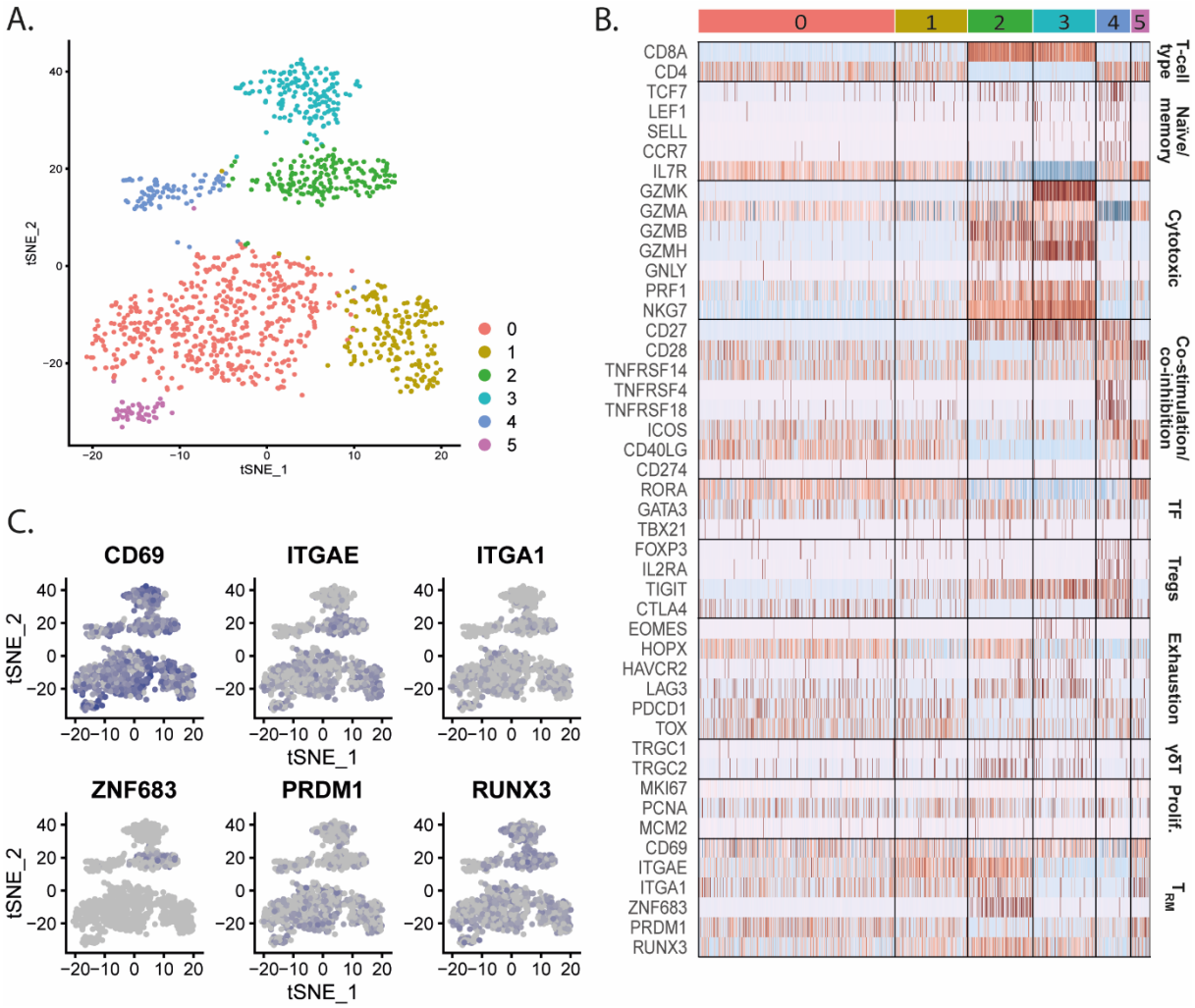

Supplemental figure 2. Selection of projected and integrated T_{RM} cells. (A) TSNE representation of unsupervised clustering of donor derived T_{RM} cells isolated intestine grafts (n=1164)[14]. (B) Heatmap displaying T cell function-associated genes expression per cluster (C) Featureplot representation of T_{RM} marker expression.

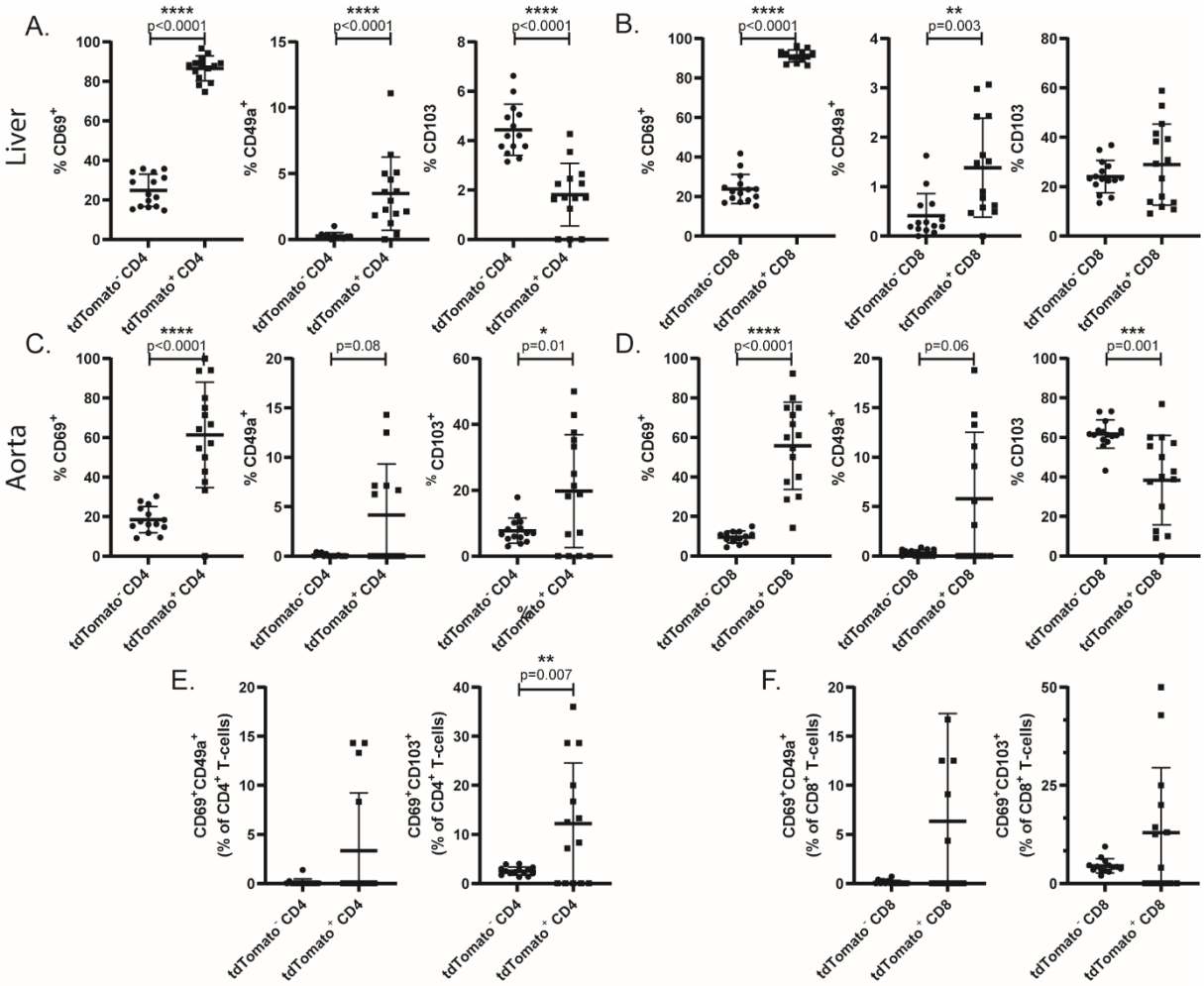

Supplemental figure 3. Plaque originating T_{RM} cells significantly upregulate CD69 and CD49α. Percentage of $CD69^+$, $CD49\alpha^+$ and $CD103^+$ $tdTomato^+$ versus $tdTomato^-$ $CD4^+$ (A) and $CD8^+$ (B) T-cells in the liver and aorta (C and D) (gated on live $CD45^+Thy1.2^+CD4^+$ or $CD8^+$ T-cells). Plots contain individual data points with mean ± SD. Significance was determined by unpaired t-test. Outliers were removed after a ROUT test.

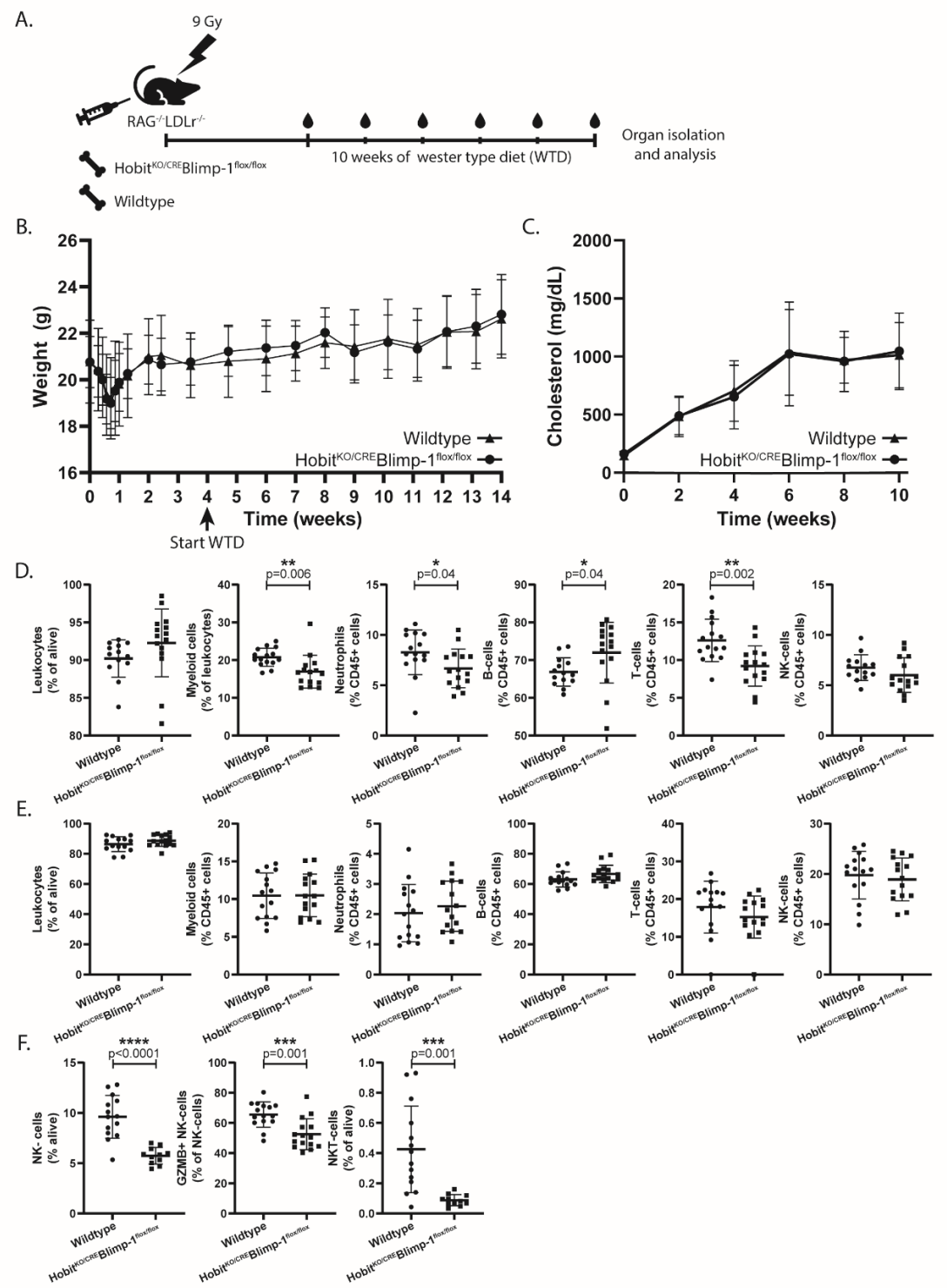

Supplemental figure 4. Effect of reduced T_{RM} formation on vitality of the mice. (A) Graphical representation of experimental set up. (B) Mouse weight during the experiment in weeks, including 4 weeks recovery time after irradiation followed by 10 weeks of western type diet (arrow indicates start of western type diet). (C) Plasma cholesterol levels of the mice during the 10 weeks of western type diet. (D) Systemic and (E) splenic immune cell levels, including leukocytes ($CD45^+$, as a percentage of live cells), myeloid cells ($CD11b^+$), Neutrophils ($CD11b^+Ly6C^+Ly6G^+$), B-cells ($CD19^+$), T-cells ($Thy1.2^+$), and NK-cells ($NK1.1^+$) as a percentage of live $CD45^+$ cells. (F) Innate lymphoid populations in the liver including NK-cells ($NK1.1^+$), GZMB+NK-cells ($NK1.1^+GZMB^+$, as a percentage of NK-cells), and iNKT-cells ($Thy1.2^+CD1dTet^+$) as a percentage of live cells. Plots contain individual data points with mean ± SD. Significance was determined by unpaired t-test. Outliers were removed after a ROUT test.

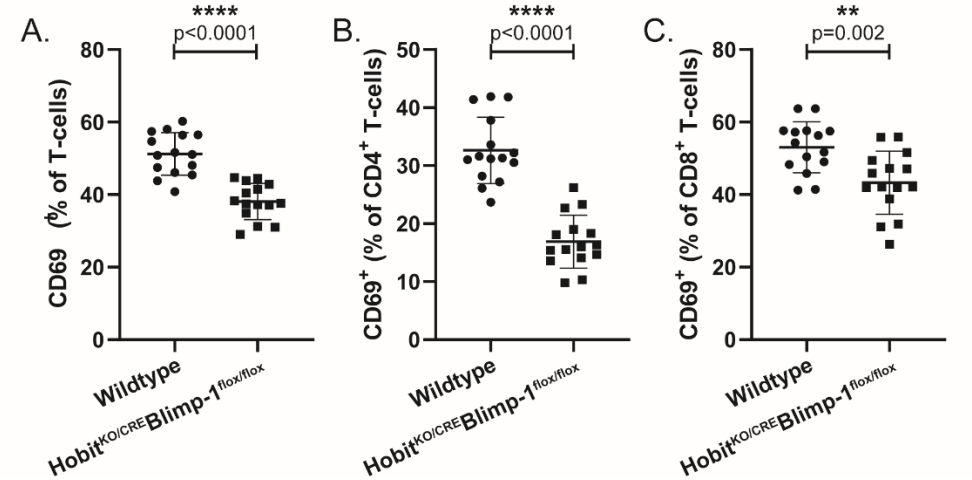

Supplemental figure 5. Livers of Hobit$^{KO/CRE}$Blimp-1$^{flox/flox}$ mice exhibit significantly reduced CD69+ T-cell levels, compared to wildtype mice. Percentage of (A) CD69$^+$ T-cells, (B) CD69$^+$CD4$^+$ T-cells, and (C) CD69$^+$CD8$^+$ T-cells, gated on live CD45$^+$ cells. Plot contain individual data points with mean ± SD. Significance was determined by unpaired t-test. Outliers were removed after a ROUT test.

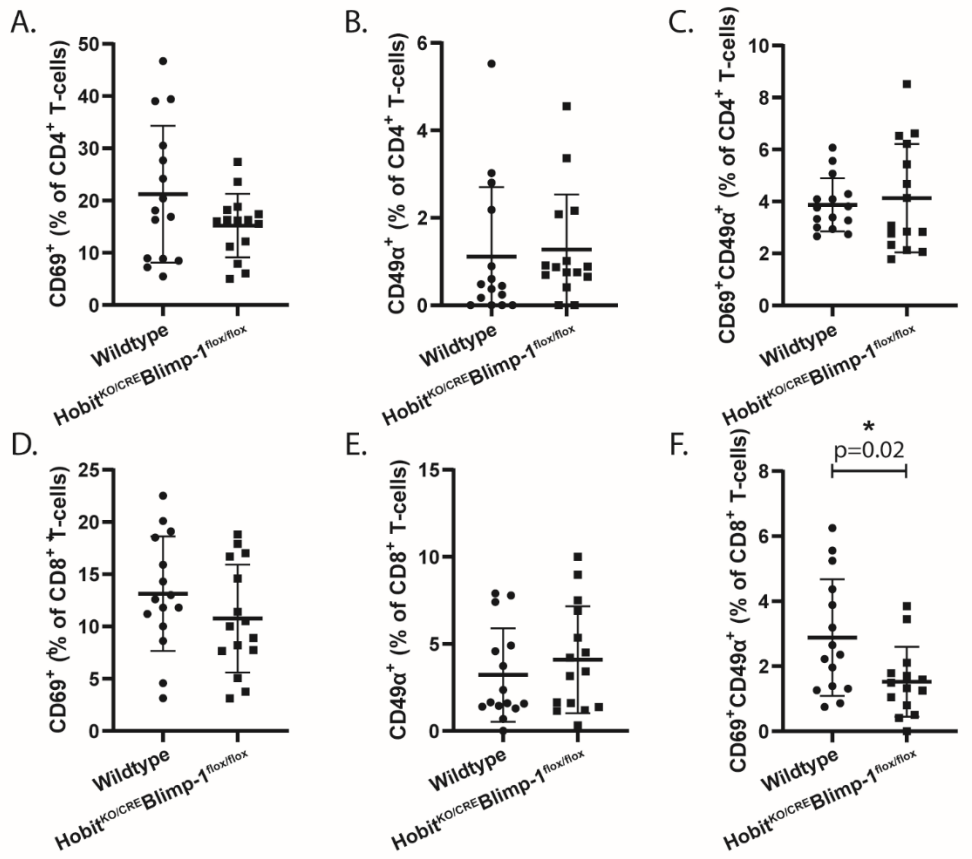

Supplemental figure 6. CD4+ and CD8+ T-cell subpopulations in the atherosclerotic lesions of Hobit$^{KO/CRE}$Blimp-1$^{flox/flox}$ mice, compared to wildtype mice. Percentage of (A) CD69$^+$, (B) CD49α$^+$, and (C) CD69$^+$CD49α$^+$CD4$^+$ T-cells, and the percentage of (D) CD69$^+$, (E) CD49α$^+$, and (F) CD69$^+$CD49α$^+$CD8$^+$ T-cells. Plot contain individual data points with mean ± SD. Significance was determined by unpaired t-test. Outliers were removed after a ROUT test.

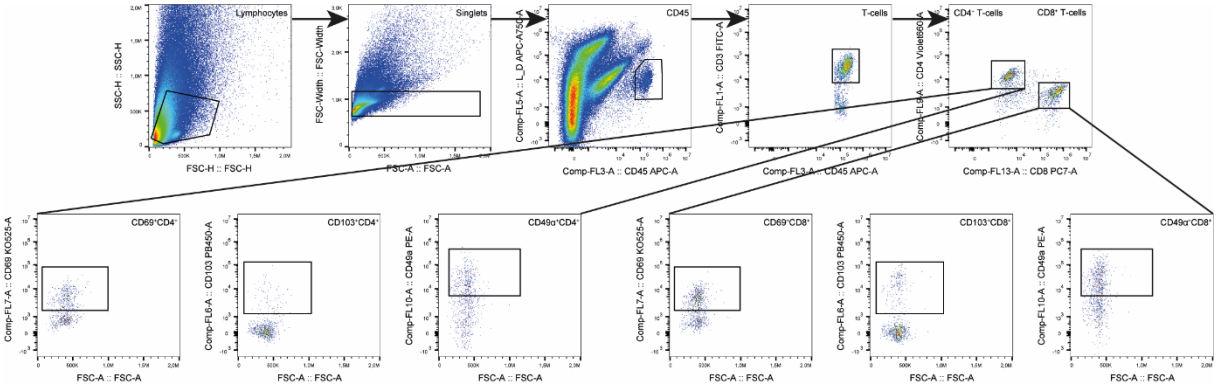

Supplemental figure 7. Flow cytometry gating strategy to evaluate T_{RM} marker expression by T-cells in human atherosclerotic lesions. $CD4^+$ and $CD8^+$ T-cells were gated on live $CD45^+CD3^+$ singlets. Within the $CD4^+$ and $CD8^+$ T-cell population the expression of CD69, CD49α and CD103 was evaluated.

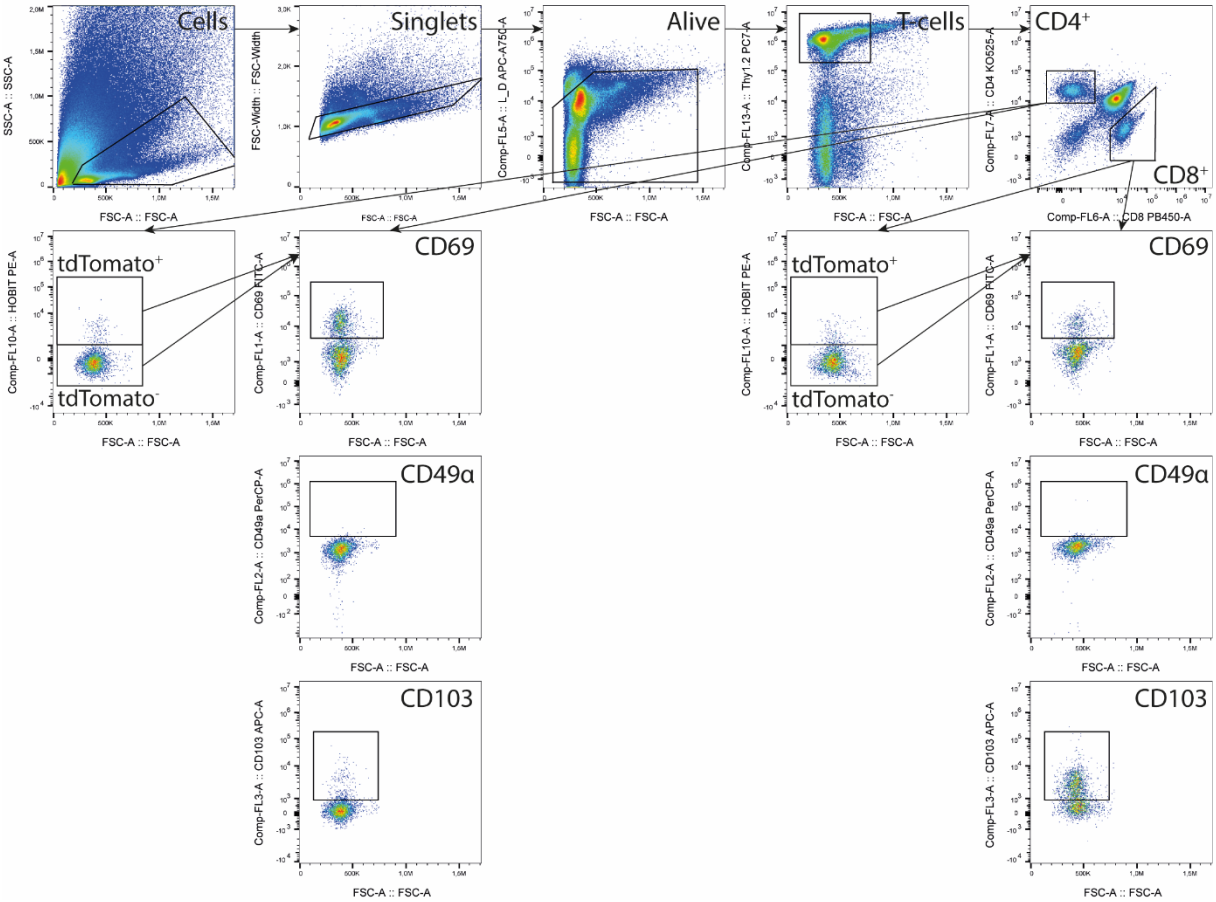

Supplemental figure 8. Flow cytometry gating strategy to identify CD69, CD103, and CD49α expression by tdTomato^{+} T-cells and tdTomato^{-} T-cells. CD4^{+} and CD8^{+} T-cells were gated on live CD45^{+} singlets. For the evaluation of CD69, CD103 and CD49α expression by tdTomato$^{+/-}$ T-cells (figure 3, figure S2), CD4^{+} and CD8^{+} T-cells were split based on tdTomato expression, followed by evaluation of CD69, CD103 and CD49α. For identification of CD69, CD103 and CD49α in Hobit$^{KO/CRE}$Blimp-1$^{flox/flox}$ mice versus wildtype mice (figure 4, figure S5), CD69, CD103 and CD49α expression was directly gated on CD4^{+} and CD8^{+} T-cells.

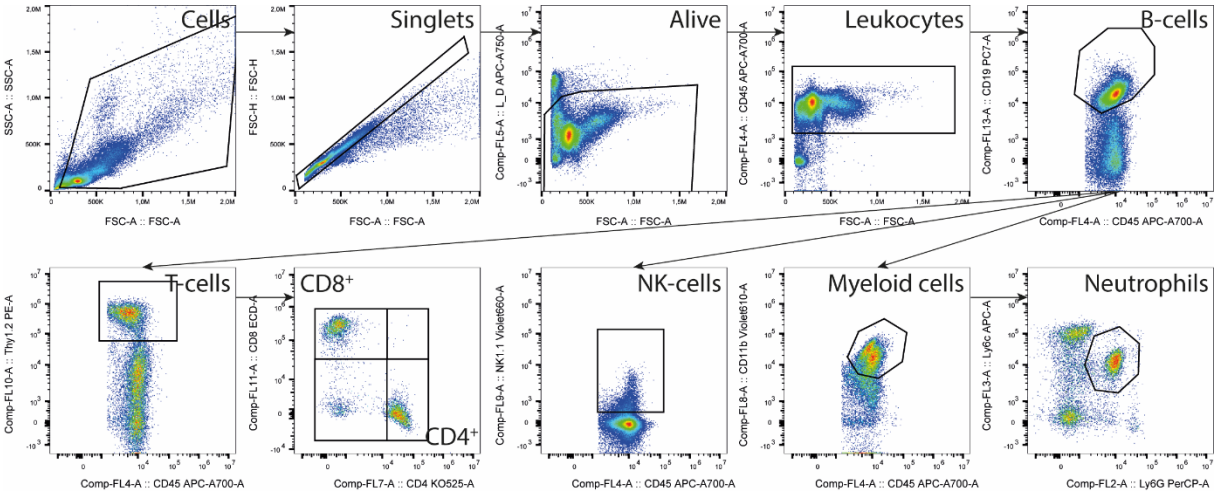

Supplemental figure 9. Flow cytometry gating strategy to identify general immune cell populations. Including leukocytes (live $CD45^+$ cells), B-cells ($CD45^+CD19^+$), T-cells ($CD45^+CD19^-Thy1.2^+$), $CD8^+$ T-cells ($CD45^+CD19^-Thy1.2^+CD8^+$), $CD4^+$ T-cells ($CD45^+CD19^-Thy1.2^+CD4^+$), NK-cells ($CD45^+CD19^-NK1.1^+$), myeloid cells ($CD45^+CD19^-CD11b^+$), and neutrophils ($CD45^+CD19^-CD11b^+Ly6C^+Ly6G^+$).

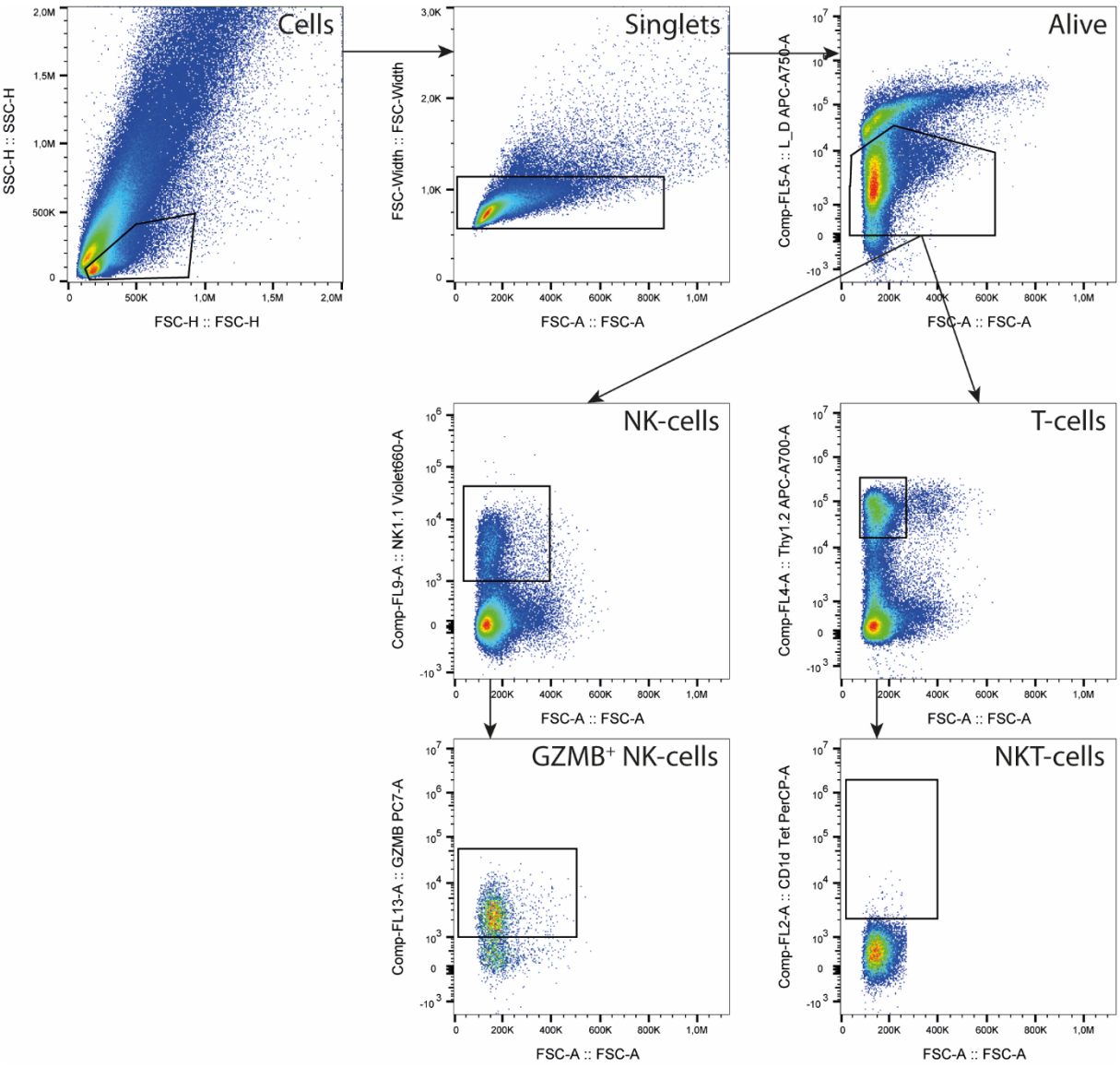

Supplemental figure 10. Flow cytometry gating strategy to identify innate lymphocyte populations. Including NK-cells (live NK1.1^{+} cells), GZMB^{+} NK-cells (GZMB^{+} NK1.1^{+} cells) and NKT-cells (live Thy1.2^{+}CD1d tetramer^{+}).

SUPPLEMENTARY TABLES

List of anti-human antibodies

Marker	Fluorochrome	Clone	Supplier	Catalog number
CD45	APC	2D1	Biolegend	368512
CD3	FITC	OKT3	BD Horizon	317306
CD4	BV650	RPA-T4	Biolegend	300536
CD8a	PE-Cy7	SK1	Biolegend	344711
CD69	BV510	FN50	Biolegend	310936
CD103	eFluor450	Ber-ACT8	Biolegend	350213
CD49a	PE	TS2/7	Biolegend	328303
eBioscience™ Fixable Viability Dye eFluor™ 780	AF780		eBioscience	65-0865-18

List of anti-mouse antibodies

Marker	Fluorochrome	Clone	Supplier	Catalog number
CD103	APC	2E7	eBioscience	17-1031-82
CD11b	BV510	M1/70	Biolegend	101245
CD11b	BV605	M1/70	Biolegend	101257
CD19	PE-Cy7	6D5	Biolegend	115519
CD1d tet	PercP-Cy5.5	L363	Biolegend	140514
CD3e	V500	500A2	BD Horizon	560771
CD4	BV510	RM4-5	Biolegend	100559
CD45	AF700	30-F11	Biolegend	506338
CD45R/B220	BV510	RA3-6B2	Biolegend	103248
CD49a	PerCP	HMalpha1	Biolegend	142611
CD69	FITC	H1.2F3	eBioscience	11-0691-85
CD8a	PE-Dazzle594	S3-6.7	Biolegend	100712
CD8a	BV450	S3-6.7	eBioscience	48-0081-82
GZMB	PEcy7	NGZB	eBioscience	25-8898-80
Ly6c	APC	HK1.4	eBioscience	17-5932-82
Ly6G	PerCP	1A8	Biolegend	127654
NK1.1	BV650	PK136	BD Horizon	564143
Thy1.2	AF700	53-2.1	Biolegend	140324
Thy1.2	PE-Cy7	53-2.1	Biolegend	140310
Thy1.2	PE	30-H12	Biolegend	105308
eBioscience™ Fixable Viability Dye eFluor™ 780	AF780		eBioscience	65-0865-18

Supplementary table 1. Antibody list.